CHARACTERIZATION OF THULIUM DOPED FIBER FOR MID INFRARED LASER APPLICATIONS

by

Wilfrid Innocent Ndebeka

Thesis presented in partial fulfilment of the
requirements for the degree of
Master of Science in Physics
at Stellenbosch University

Supervisor: Prof. Erich Rohwer
Co-Supervisor: Prof. Heinrich Schwoerer,
Faculty of Sciences
Physics Department
March 2011

Declaration

By submitting this thesis electronically, I declare that the entirety of the work contained therein is my own, original work, that I am the sole author thereof (save to the extent explicitly otherwise stated), that reproduction and publication thereof by Stellenbosch University will not infringe any third party rights and that I have not previously in its entirety or in part submitted it for obtaining any qualification.

Date: March 2011

Abstract

High output power sources producing output in the so-called "eye-safe" 2 μm spectral region have recently shown much promise for a number of applications. The 2 μm radiation produced by the $^3F_4 - ^3H_6$ transition of Tm^{3+} has many applications in medical, commercial, and military technologies. The strong absorption of radiation at this wavelength by water and human tissues is attractive for laser surgery, while the low atmospheric and “eye-safe“ properties make this system useful for materials processing, range-finding, remote sensing, and other applications. Generally, the Mid-Infrared ($3 - 5$ μm) spectral region is of interest and 2 μm devices also provide an ideal starting wavelength. In this work, the spectral characteristics of a special Tm^{3+}-doped fiber, produced by a Canadian company (CorActive), is investigated. The fiber is pumped with a commercially pump diode laser operating at 800 nm. The dependence of the fiber's slope efficiency on different cooling techniques is investigated experimentally. With a 4-m-long fiber, 5 W multi-mode continuous wave (CW) output is generated for 20 W of absorbed power, with a slope efficiency of 53.6%. A spectral output with multi-wavelengths ranging from $2.01 - 2.04$ μm is obtained.

Opsomming

Hoë drywing bronne wat uitset in die so-genaamde 'oog-veilige' 2 μm spektrale gebied lewer het onlangs baie belofte begin toon vir 'n verskeidenheid van toepassings. Die 2 μm straling wat deur die $^3F_4$-$^3H_6$ oorgang van Tm^{3+} geproduseer word het baie toepassings in mediese, kommersiële en militêre tegnologieë. Die sterk absorbsie van straling van hierdie golflengte deur water en menslike weefsel is aanloklik vir laserchirurgie, terwyl die lae atmosferiese en 'oog-veilige' aspekte die sisteem aantreklik maak vir materiaal-prossesering, afstand-bepaling, afstand-waarneming en ander toepassings. In die algemeen is mid-infrarooi spektrale gebied ($3 - 5$ μm) van belang en 2 μm toestelle bied 'n ideale begin-golflengte. In hierdie werk word die spektrale eienskappe van 'n spesiale Tm^{3+} gedoteerde vesel, geproduseer deur 'n Kanadese maatskappy (CorActive), ondersoek. Die afhanklikheid van die vesel se hellingseffektiwiteit op verskillende verkoelings tegnieke is eksperimenteel ondersoek. Met 'n 4 m lang vesel is 5 W multi-mode kontinue golf uitset gegenereer vir 20 W geabsorbeerde drywing, met 'n hellingseffektiwiteit van 53.6%. 'n Spektrale uitset met veelvuldige golflengtes wat strek van $2.01 - 2.04$ μm is verkry.

Acknowledgements

Without you God this work would not be possible.

It is with immense pleasure and gratitude that I acknowledge the support, motivation, and help of my supervisors Professor Erich Rohwer and Professor Heinrich Schwoerer.

I would also address my gratitude to Professor Hubertus Von Bergmann and Dr Christine Steenkamp for their input during the LRI technical meetings.

I am indebted to Alexander Heidt for all the assistance he gave me for the accomplishment of this work.

Special thanks to Mr U.G.K Deutschländer and Mr J. M. Germishuizen for always being available for technical matters.

I will not forget Eben Shield for his help on electronic matters.

It gives me also great pleasure in acknowledging the support and inspiration of all L.R.I. and O.S.A. members.

I would also like to acknowledge the African Institute for Mathematical Sciences (AIMS), the University of Stellenbosch and the African Laser Centre (ALC) for funding my MSc studies.

My profound gratitude goes also to my family, parents, and friend for their support and love

Thank you so much to all of you!!!

Contents

List of Figures

List of Tables

Chapter 1

Introduction

1.1 Motivation

Recent advances in fiber technology have produced demonstrations of high power fiber lasers that can generate output power of several kilowatts. Thulium (Tm)-doped fiber lasers are beginning to emerge as the latest revolution in high-power fiber technology [5]. Operating at $1.9 - 2.1$ μm, this technology falls into the “eye-safer“ category of lasers giving it potential advantages over 1 μm lasers for industrial and military directed energy applications. To date, the highest power devices have been based on Ytterbium (Yb^{3+})-doped silica fibers operating around 1 μm. Lasers in this wavelength region are serious eye hazard since their beams are invisible but the power can be imaged onto the retina. The success of Yb-doped fiber technology is primarily owed to two main factors: the low quantum defect associated with this system and the abundance of high-brightness pump sources at $915 - 975$ nm. The low quantum defect leads high efficiency operation and low thermal loading of the fiber. The Ytterbium sensitized erbium (Er:Yb) fibers operating at ~ 1.55 μm have been the traditional choice for eye-safer fiber laser applications. The quantum defect for (Er:Yb) system indicates that efficiencies approaching 60% is possible, very few demonstrations have shown greater than 40% to date. At present, the power scaling of thulium-(Tm)-doped fiber lasers, emitting in the so-called "eye-safe" wavelength is investigated. Tm-doping is especially interesting for high power laser operations due to the possibility of a cross relaxation or "two-for-one" phenomenon, in which two excited Tm ions can be produced with only one pump photon [6]. Thus, in theory one can obtain a

maximum slope efficiency of 80%, if pumping at 800 nm, which increases the power scaling possibilities due to reduced heat extraction problems [7]. The comparison on the progress of 1, 1.5 and 2 μm laser technology is shown in Figure (1.1). Figure (1.1) shows that the power scaling of Tm-doped fiber lasers has rapidly gained momentum and now exceeds Er: Yb technology [8]. The main motivation for development of high-power 2 μm systems

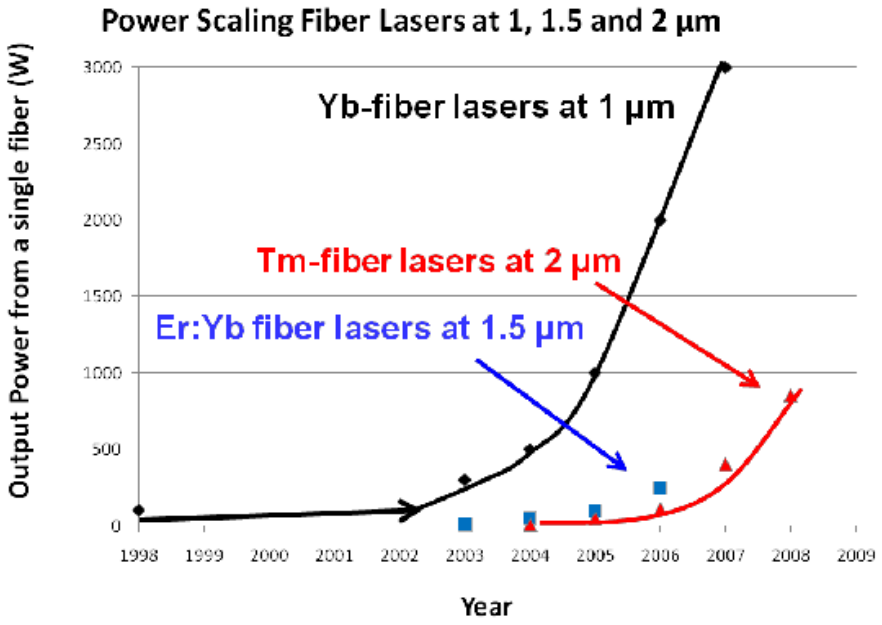

Figure 1.1. Power scaling of Tm-doped fiber [1]

has been for applications which would benefit from operating at eye-safer wavelengths, where permissible free space transmission levels can be several order of magnitude greater than at 1 μm. Military deployment of laser weapons systems could certainly find wider acceptance if the systems operated at eye-safer wavelengths. Pulsed laser systems may be used either for direct applications such LIDAR and range finding, or for conversion into the mid- and far-IR for countermeasures, remote sensing, and spectroscopy. In the medical market, Tm-doped fiber lasers present a potential alternative to current generation CW solid-state 2 μm lasers [9, 10].

1.2 Aim

The main aim of the experimental work documented in this thesis is to investigate a newly developed "triple-clad" Tm-doped fiber manufactured by the Canadian company CorActive, and investigate the occurrence of the cross relaxation process in dependence of different cooling methods, and also to implement a Tm- doped fiber laser, operating at 2 μm, at the Laser Research Institute. CorActive produces a wide range of specialty fiber products including rare-earth doped single clad, double clad, and triple clad, attenuating, UV sensing, and Mid- to Far- IR fibers.

1.3 Outline of thesis

A background review on the propagation of light through an optical fiber is presented in Chapter 2. Descartes laws or the laws of reflection and refraction, and the condition of total internal reflection between two media are described in Section 2.2.2. The explanation of propagation of light as ray theory or mode theory is presented in Sections 2.2.3 and 2.2.5, respectively. Sections 2.2.7 and 2.2.8 present the different types of fibers. The properties of optical fiber transmission is presented in Section 2.3.

A brief literature study on rare earth ions with their electronic and optical properties is the subject of Chapter 3. Section 3.3 presents the revolution in high-power fiber lasers with thulium-(Tm)-doped fiber lasers which are beginning to emerge as the latest revolution in laser technology.

Chapter 4 is dedicated to the experimental setups and techniques used during the characterization of Tm-doped fiber. As part of the preliminary study, the characterizations on the pump diode, mirrors, and the preparation of the Tm-doped fiber, which will be used as active medium of the laser cavity, are described in Sections 4.2.2, 4.4, and 4.5, respectively. The diffraction grating and the calibration of the grating monochromator for the measurement of the spectral output are presented in Sections 4.7 and 4.8, respectively. Section 4.9 describe the experimental methods used for the measurements of the efficiencies and spectra of the Tm-doped fiber using different cooling techniques.

The experimental results studied in Chapter 4 are presented in Chapter 5. The result of the diode efficiency and spectral intensity, and the variation of wavelength with current are presented in Section 5.1. The transmission result of the mirrors used for laser cavity and the results of the measurements of efficiencies and spectra of the fiber by using different cooling methods are presented in Sections 5.2 and 5.5.1, 5.5.2, respectively.

Chapter 6 presents a summary and conclusion to the results of the experimental work and proposals for future work and suggestions for improvements are given.

Chapter 2

Propagation of light through an optical fiber

Optical instruments make use of light that is transmitted between different locations in the form of beams that are collimated, relayed, focused or scanned by mirrors, lenses and prisms. Diffracted and broadened beams can be refocused by the use of lenses and prisms, but such beams are easily obstructed or scattered by diverse objects. There exists a new technology of transmitting light through dielectric conduits: *waveguide optics*.

In this chapter the basic properties of propagation of light along an optical fiber will be discussed, and the fiber properties such as attenuation and dispersion will be discussed in section 2.3.

2.1 Waveguides

An optical waveguide is a spatially inhomogeneous dielectric structure for guiding light, i.e. it is restricting the spatial region in which light can propagate. An optical waveguide consists of slab, strip, or cylindrical dielectric material, surrounded by another dielectric material of lower refractive index. Light is conducted through the inner medium without radiating into the surrounded medium. Waveguides are widely used in optical fibers, which are made, in general, with two concentric cylinders of low-loss dielectric material such as glass. Optical waveguides are divided into two categories:

• Rectangular waveguides, which are used in integrated optics; and

• Cylindrical waveguides, which are used to make optical fibers.

The study of the fiber will be focused on the latter case: cylindrical waveguides

2.2 Optical fibers

In simple terms, an optical fiber is a cylindrical dielectric waveguide made of low-loss materials such as silica glass, through which light can be transmitted by successive internal reflections.

An optical fiber consists of three parts: the core, the cladding, and the coating or buffet. The simple structure of the fiber is shown in Figure (2.1). The *core* is a cylindrical rod of dielectric material, with a radius **a** and an index of refraction n_1. The core is surrounded by a layer of low refractive index n_2 ($n_2 < n_1$) with a radius **b** called *cladding*. The core and the cladding are generally made of glass. Light propagates principally along the core of the fiber. The cladding reduces loss of light from the core into the surrounding air, reduces scattering loss at the surface of the core, protects the fiber from absorbing surface contaminants, and adds mechanical strength. Nowadays we find double-clad fibers (DCF) and Triple-clad fibers (TCF). To protect the fiber of physical damages, the cladding is enclosed in an additional layer called *coating* or *buffer*, which is a typically a polymer.

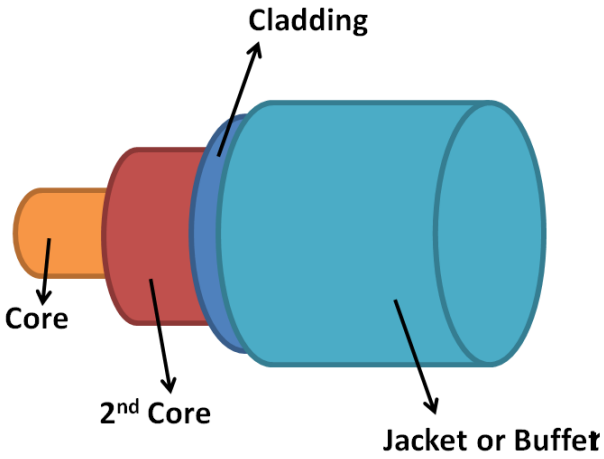

Figure 2.1. Basic structure of an optical fiber

2.2.1 Propagation of light in an optical fiber

Total internal reflection is the basic phenomenon responsible for guiding light in an optical fiber. The propagation and the transmission of light along an optical fiber can be described by two theories. First, light is described as simple ray (Ray Theory of light) or geometrical optics approach, and the second theory is that light is described as an electromagnetic wave (Mode Theory). The ray theory is used to approximate the light acceptance and guiding properties of an optical fibers. The mode theory describes the behavior of light within an optical fiber and it is useful in describing the optical fiber properties of absorption, attenuation and dispersion. The propagation of light into an optical fiber follows Descartes laws: reflection and refraction.

2.2.2 Reflection and refraction of light at the boundary between two Media

The reflection and refraction phenomena will be described by using the ray theory or geometrical optics approach.

Reflection

When a ray approaches a reflecting surface, such as a mirror, the ray that strikes the surface mirror is called the *incident* ray, and the one that bounces back is called the *reflected* ray. An imaginary line perpendicular to the point at which the incident ray strikes the reflecting surface is called *normal* or *perpendicular*. The angle between the incident ray and the normal is called the *angle of incidence*, and the one between the reflected ray and the normal is called the *angle of reflection* (Figure 2.2a). Each reflected ray will be reflected back at the same angle as the incident ray, the path of the ray reflected from the surface forms an angle equal to the one formed by its path in reaching the medium. The law of reflection states that "the angle of incidence is equal to the angle of reflection $(i = r)$"

Index of refraction

The index of refraction or the refractive index of a transparent optical medium, is a measure of how much the speed of light is reduced inside the medium. The index of refraction is

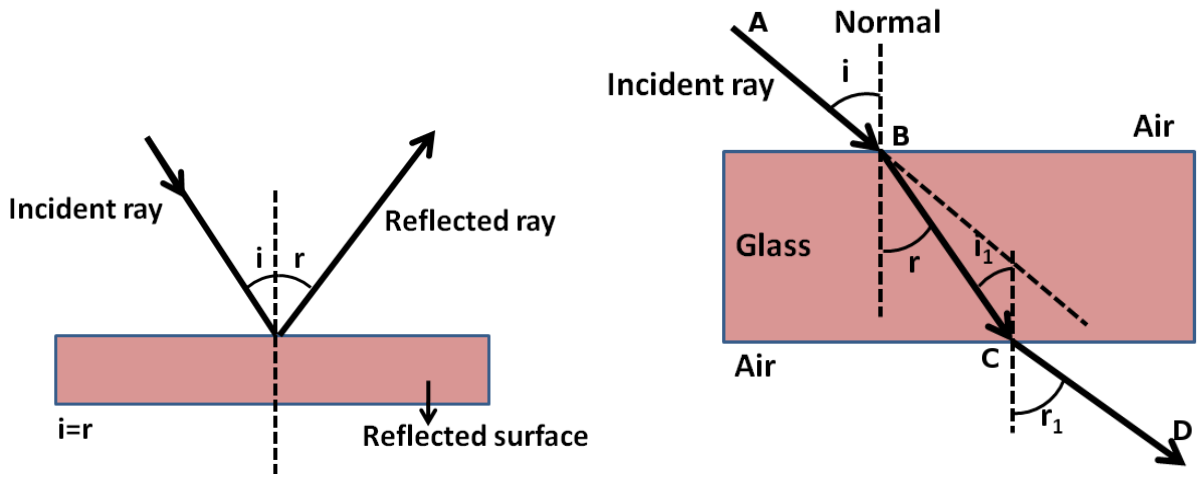

(a) Reflection (b) Refraction

Figure 2.2. Reflection and Refraction of light

given by

$$n = \frac{c_0}{v}, \tag{2.1}$$

where c_0 is the speed of light in free space (vacuum) is 3×10^8 m/s and v is the speed of light when it travels inside the medium. Typical refractive index values for glasses and crystals (e.g. laser crystals) in the visible spectral region are in the range form $1.4 - 2.8$, and typically the refractive index increases for short wavelengths.

Refraction of light

When a light passes from one medium, with the index of refraction n_1, into a medium of refractive index n_2, a change in the direction of the ray will occur. This change of direction as the ray enters the second medium is called *refraction*. As the ray passes through the boundary, it is bent either toward ($n_1 < n_2$) or it is bent away ($n_1 > n_2$) from the normal. The angle between the normal and the path of the ray through the second medium is the *angle of refraction* (Figure 2.2b). The ray moves from point A to point B at a constant speed. This is the incident ray; as it penetrates the glass boundary at point B, the velocity of the ray is slowed down. This causes the ray to bend toward the normal. The ray takes the path from point B to point C through the glass and becomes both the refracted ray from the top surface and the incident ray to the lower surface. The ray passes then from the glass to the air (second boundary), it is again refracted away from the normal, and

takes the path from point C to point D.

According to Snell's law (also known as Descartes' law, the Snell-Descartes law, and the law of refraction), the relationship between the angles of incidence and refraction, when referring to light or other waves passing through a boundary between two different isotropic media with refractive indices n_1 and n_2, respectively, is given by

$$\frac{\sin\theta_1}{\sin\theta_2} = \frac{n_2}{n_1} = \frac{v_1}{v_2} \quad \text{or} \quad n_1 \sin\theta_1 = n_2 \sin\theta_2, \tag{2.2}$$

where θ_1 and θ_2 are the angles of incidence and refraction, respectively, and v_1 and v_2 are the velocities of propagation of light in the two media.

Total internal reflection

For $n_1 > n_2$, the angle of refraction is greater than the angle of incidence, $\theta_2 > \theta_1$, so that as θ_1 increases, θ_2 reaches 90°(see Figure 2.3). This occurs when $\theta_1 = \theta_c$ (the critical angle). According to Snell's law, we have

$$n_1 \sin\theta_c = n_2 \sin\frac{\pi}{2} = n_2 \quad \text{so that} \quad \theta_c = \sin^{-1}\left(\frac{n_2}{n_1}\right) \tag{2.3}$$

When $\theta_1 > \theta_c$, Snell's law cannot be satisfied and refraction does not occur. The incident ray is totally reflected as if the surface was a perfect mirror [11]. The phenomenon of total internal reflection is the basis of propagation of light along a fiber.

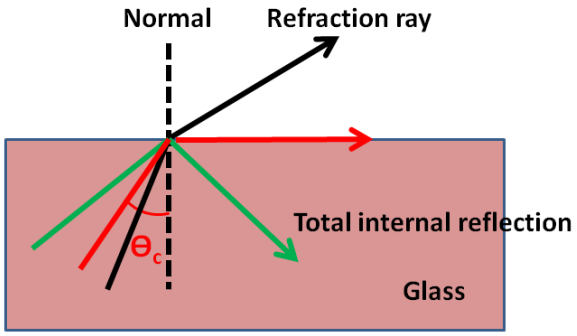

Figure 2.3. Illustration of total internal reflection of light between two media when the incident angle of the incident light is greater than the critical angle.

2.2.3 Ray theory

Two types of rays can propagate along an optical fiber:

- Meridional rays; and
- Skew rays.

The meridional rays are rays that pass through the axis of an optical fiber and are used to illustrate the basic transmission properties of an optical fibers. Skew rays are rays that travel through an optical fiber without passing through its axis [11].

Meridional rays

Meridional rays can be classified in two types of rays: bound and unbound rays. Bound rays remain in the core and propagate along the axis of the fiber by *total internal reflection*. Unbound rays are refracted out of the fiber core. Figure 2.4 shows the possible path taken

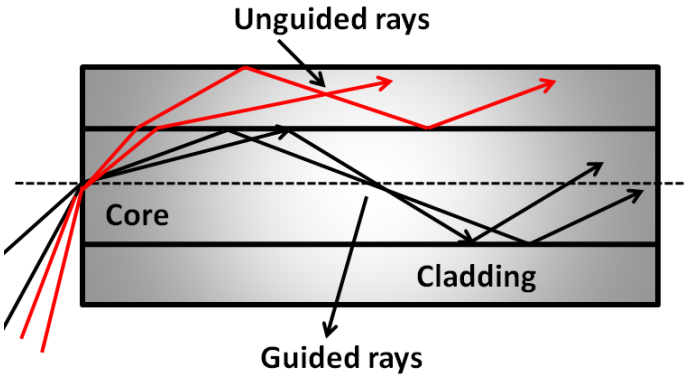

Figure 2.4. Illustration of guided and unguided rays through a step-index fiber. Guided rays propagate by total internal reflection along the core, while unguided rays are lost in the cladding.

by bound (or guided) and unbound (or unguided) rays in a step index fiber.

A step-index profile is a refractive index characterized by uniform refractive index within the core and sharp decrease in refractive index at the core-cladding interface (Figure 2.5).

Bound rays propagate in fibers due to total internal reflections, so the question is how do

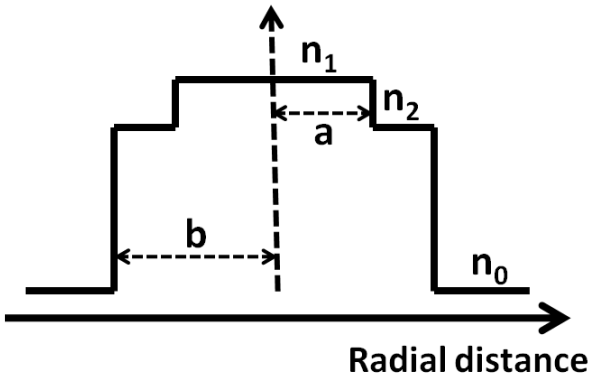

Figure 2.5. Step-index profile of an optical fiber

these light rays enter the fiber?

An optical ray is guided by total internal reflections within the fiber if its angle of incidence on the core-cladding interface is greater than the critical angle θ_c as defined in equation (2.3), and remains inside the core as it is reflected. Only rays striking the core-cladding interface, with angles greater than the critical angle θ_c, will propagate along the fiber. The incident ray I_1 enters the fiber at the angle θ_a. I_1 is refracted upon entering the fiber and is transmitted to the core-cladding interface at angles greater than the critical angle θ_c. I_1 is totally reflected back into the core and continues to propagate along the fiber. The incident ray I_2 enters the fiber at an angle greater than θ_a. Again I_2 is refracted upon entering the fiber and is transmitted to the core -cladding interface. I_2 strikes the core-cladding interface at an angle less than the critical angle θ_c. I_2 is refracted into the cladding where it will be lost as shown in Figure 2.6. Unguided rays are rays striking the core-cladding interface with angles less than the critical angle θ_c.

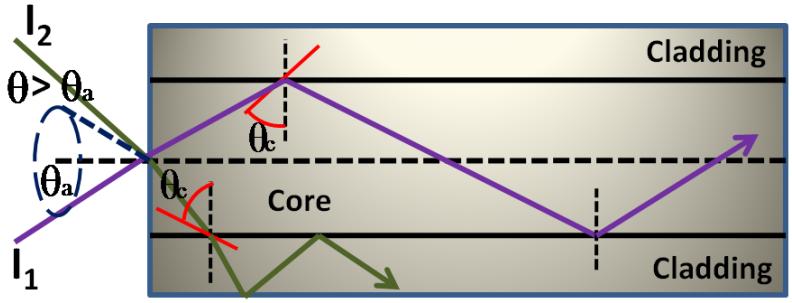

Figure 2.6. How light enters an optical fiber

Rays striking the core-cladding interface at angles precisely equal to the critical angle will be refracted tangentially to the core-cladding boundary at the point of incidence. Light ray incident on the fiber core will propagate along the fiber if it is within the *acceptance cone* define by the angle θ_a shown in Figure 2.7, where θ_a is the acceptance angle and is defined as the maximum angle, to the axis of the fiber, that light entering the fiber is propagated. The acceptance angle is related to the refractive indices of the core and cladding, and with the medium surrounding the fiber. This relationship is called *numerical aperture* of the fiber.

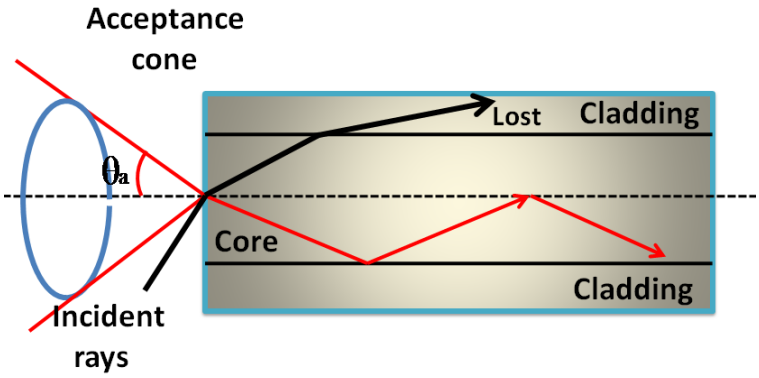

Figure 2.7. Fiber acceptance cone

Skew rays

Skew rays are rays propagating along the fiber without passing throug the center axis of the fiber (Figure 2.8). Skew rays tend to propagate near the edge of the fiber core. The acceptance angle for skew rays is larger than the acceptance angle of meridional rays. Skew rays are often used in the calculation of light acceptance in optical fiber.

2.2.4 Numerical aperture of an optical fiber

By definition, the numerical aperture NA is a measurement of the ability of an optical fiber to capture light. The NA is also used to define the acceptance cone of an optical fiber.

Using the geometry of Figure 2.6, and applying Snell's law at the air-core interface, we have

$$n_0 \sin\theta_a = n_1 \sin\left(\frac{\pi}{2} - \theta_c\right) = n_1 \cos\theta_c \tag{2.4}$$

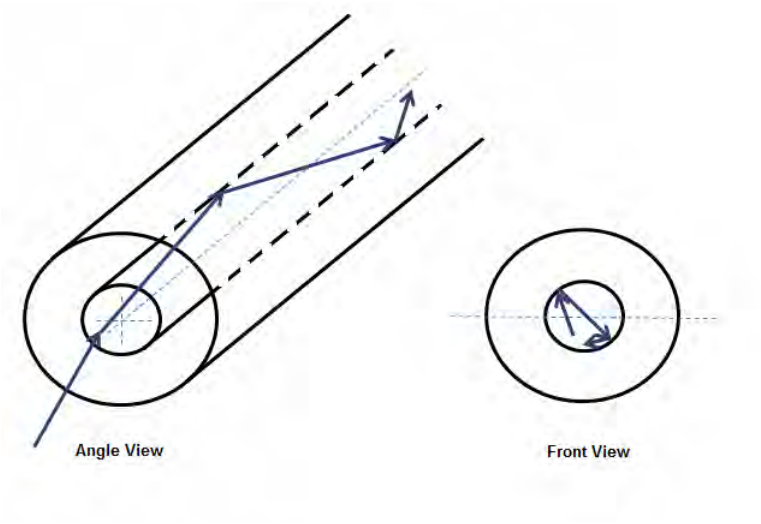

Figure 2.8. Path taken by skew ray in an optical fiber

Squaring both sides, we get, for $n_1 < n_2$

$$n_0^2 \sin^2\theta_a = n_1^2\left(1 - \sin^2\theta_c\right) = n_1^2\left(1 - \frac{n_2^2}{n_1^2}\right)$$

Thus,

$$n_0 \sin\theta_a = \left|n_1^2 - n_2^2\right|^{\frac{1}{2}} \tag{2.5}$$

Equation 2.5 has the same form as the numerical aperture in other optical systems (NA=$n\sin\theta$), like with lenses. It has become common to define the numerical aperture NA of any type of fiber to be

$$\mathrm{NA} = \sin\theta_a = \frac{1}{n_0}\left(n_1^2 - n_2^2\right)^{\frac{1}{2}} \tag{2.6}$$

θ_a is the acceptance angle, n_0, n_1, and n_2 are the refractive indices of the air, the core, and the cladding, respectively. Since $n_0 = 1$, the numerical aperture of the fiber is simply the sine of the maximum angle of incident ray with respect to the fiber axis, so that the transmitted beam is guided in the core.

For $n_1 \approx n_2$, the numerical aperture can be approximated

$$\mathrm{NA} = \left(n_1^2 - n_2^2\right)^{\frac{1}{2}} = n_1\left[\left(1 - \frac{n_2}{n_1}\right)\left(1 + \frac{n_2}{n_1}\right)\right]^{\frac{1}{2}} = n_1\left(2\Delta\right)^{\frac{1}{2}} \tag{2.7}$$

where $\Delta = (n_1 - n_2)/n_1$ is the fractional index change at the core-cladding interface.

The numerical aperture defines the maximum acceptance angle to admit and transmit light by a fiber. Lenses can be used to focus light at the input and/or output end. It is used to measure source-to-fiber coupling efficiencies. A high NA indicates a high source-to-fiber coupling efficiency.

2.2.5 Mode theory

The mode theory describes the propagation of light along a fiber using electromagnetic wave behavior from Maxwell's equations and the boundary conditions imposed by the cylindrical dielectric core and cladding. The solutions of Maxwell's equations are called *modes*.

Maxwell's equations

In free space, the electric and magnetic field satisfying Maxwell's equations are given by

$$\nabla.\mathbf{E} = 0 \tag{2.8a}$$

$$\nabla.\mathbf{B} = 0 \tag{2.8b}$$

$$\nabla \times \mathbf{E} = -\frac{\partial \mathbf{B}}{\partial t} \tag{2.8c}$$

$$\nabla \times \mathbf{B} = \mu_0 \epsilon_0 \frac{\partial \mathbf{E}}{\partial t} \tag{2.8d}$$

where the constants ϵ_0 and μ_0 are, respectively, the permittivity of free space and permeability of free space. $\mathbf{E}$ and $\mathbf{B}$ are the electric and magnetic fields, respectively.

The Wave equation

A necessary condition for $\mathbf{E}$ and $\mathbf{B}$ to satisfy Maxwell's equations is that each of their components satisfy the wave equation given by

$$\nabla^2 U - \frac{1}{c_0^2} \frac{\partial^2 U}{\partial t^2} = 0 \tag{2.9}$$

where

$$c_0 = \frac{1}{\sqrt{\epsilon_0 \mu_0}}$$

is the speed of light in vacuum, and the scalar function $U(r,t)$ represents any of the three

components of **E** and **B**.

For monochromatic electromagnetic waves in an optical medium, all components of electric and magnetic fields are harmonic functions of time with the same frequency $\omega = 2\pi\nu$. In the complex notation

$$\mathrm{E(r,t)} = Re\{E(r)\exp(j\omega t)\} \tag{2.10a}$$

$$\mathrm{B(r,t)} = Re\{B(r)\exp(j\omega t)\} \tag{2.10b}$$

where $E(r,t)$ and $B(r,t)$ represent the electric and magnetic field complex-amplitude, respectively [11].

Substituting equation 2.10 into equation 2.9, we get the Helmholtz equation

$$\nabla^2 U + k^2 U = 0 \quad \text{Helmholtz equation} \tag{2.11}$$

where $k = nk_0 = n\frac{\omega}{c_0}$ is the wavenumber,

$$c = \frac{c_0}{n}$$

and the scalar function U represents the complex amplitude of any of the three components of E and B.

In cylindrical coordinates $U = U(r, \Phi, z)$, the Helmholtz equation is given by

$$\frac{\partial^2 U}{\partial r^2} + \frac{1}{r}\frac{\partial U}{\partial r} + \frac{1}{r^2}\frac{\partial^2 U}{\partial \Phi^2} + \frac{\partial^2 U}{\partial z^2} + n^2 k_0^2 U = 0. \tag{2.12}$$

For a wave traveling in the z-direction with a propagation constant β, periodic of the angle Φ with period 2π, and assuming that the dependence of Φ is unique, U can be written as

$$U(r, \Phi, z) = u(r)e^{-jl\Phi}e^{-j\beta z}, \quad l = 0, \pm 1, \pm 2, ... \tag{2.13}$$

Equation 2.13 into equation 2.12, gives

$$\frac{d^2 u}{dr^2} + \frac{1}{r}\frac{du}{dr} + \left(n^2 k_0^2 - \beta^2 - \frac{l^2}{r^2}\right) u = 0 \tag{2.14}$$

Since

$$n = n_1 \quad \text{in the core} \quad (r < a) \tag{2.15a}$$

$$n = n_2 \quad \text{in the cladding} \quad (r > a) \tag{2.15b}$$

then, equation 2.14 can be written in the core and cladding separately

$$\begin{cases} \frac{d^2u}{dr^2} + \frac{1}{r}\frac{du}{dr} + \left(k_T^2 - \frac{l^2}{r^2}\right) = 0 \quad \text{for } r < a \text{ (core)}, \\ \\ \frac{d^2u}{dr^2} + \frac{1}{r}\frac{du}{dr} - \left(\gamma^2 + \frac{l^2}{r^2}\right) = 0 \quad \text{for } r > a \text{ (cladding)}, \end{cases} \tag{2.16}$$

where $k_T^2 = n_1^2 k_0^2 - \beta^2$ and $\gamma^2 = \beta^2 - n_2^2 k_0^2$, where β is the propagation constant and $\beta = \frac{2\pi}{\lambda}$

Equations 2.16 are the differential equations whose solutions are the familly Bessel functions. The bounded solutions are

$$u(r) \propto \begin{cases} J_l(k_T r), & r < a \text{ (core)} \\ K_l(\gamma r), & r > a \text{ (cladding)}. \end{cases} \tag{2.17}$$

where $J_l(k_T r)$ is the Bessel function of the first kind and order l, and $K_l(\gamma r)$ is the modified Bessel function of the second kind and order l. k_T and γ determine the rate of change of $u(r)$ in the core and in the cladding, respectively. The bounded solutions J_l and K_l are the modes traveling in an optical fiber and are said to be transverse. The transverse mode propagate along the axis of the fiber [11]. There are two types of transverse modes:

- the Transverse Electric modes (TE);

- the Transverse Magnetic modes (TM).

In the TE modes, the electric field vector is perpendicular to the direction of propagation and the magnetic field vector is in the direction of propagation. In the TM modes, the magnetic field is perpendicular to the direction of propagation, the electric field is in the direction of propagation.

2.2.6 Normalized frequency or V-parameter

The normalized frequency or V parameter determines how many modes a fiber can support. The Normalized frequency is given by

$$\mathrm{V} = \frac{2\pi \mathbf{a}}{\lambda_0} \left(n_1^2 - n_2^2\right)^{\frac{1}{2}}, \tag{2.18}$$

where λ_0 is the wavelength of the light and **a** the core radius [11, 12].

The relationship between the number of modes that an optical fiber can support and the V parameter is given by

$$M = \frac{4}{\pi^2}\mathrm{V}^2 \quad \text{for V} \ggg 1. \tag{2.19}$$

2.2.7 Single mode fibers

In single mode fibers, V $<$ 2.405 [11] and only one mode propagates along the fiber. Single mode fibers propagate the fundamental mode in the core, while high order modes are lost in the cladding. Single mode operation is achieved by using small core diameter and small numerical aperture (making n_2 close to n_1), or by operating at sufficiently long wavelengths. The fundamental mode has a bell-shaped spatial distribution similar to the Gaussian distribution (Figure 2.9a). In a single mode fiber, there is only one mode with one group velocity, so that a short pulse of light arrives without delay distortion. Referring on many optics books, single mode fibers have a lower signal loss and higher information capacity (bandwidth).

2.2.8 Multimode fibers

Multimode fibers propagate more than one mode. The output of multimode fibers is a superposition of all guided mode (Gaussian beams of order m and n), and are called Transverse Electro-Magnetic LP_{mn} (Figure 2.9b), the number of modes propagated depends on the core size and the numerical aperture (NA). As the core size and NA increase, the number of modes increases. A large core size and higher NA have several advantages: light is launched into a multimode fiber with more ease. The higher NA and the larger core

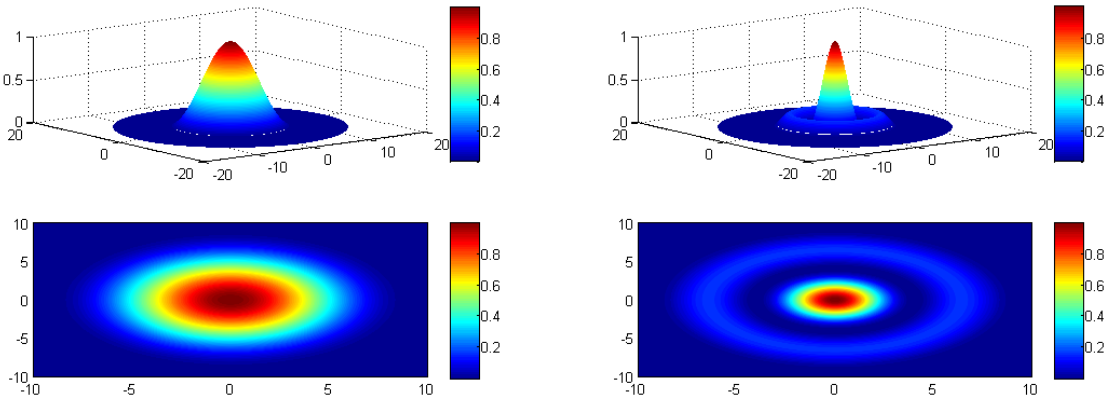

(a) Single mode (LP_{01}) (b) LP02 mode

Figure 2.9. Lower modes propagating inside the fiber [2]

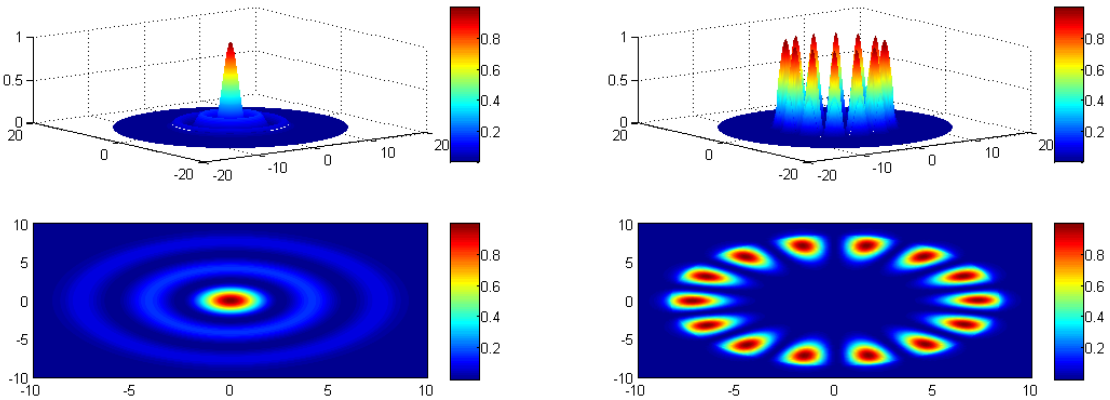

(a) LP_{03} mode (b) LP_{71} mode

Figure 2.10. Higher mode intensity distributions in multimode fibers [2]

size make it easier to make fiber connections. During fiber splicing, core-to-core alignment becomes less critical.

Multimode fibers also have some disadvantages. As the number of modes increases, the effect of modal dispersion increases. Modal dispersion (intermodal dispersion) means that modes arrive at the fiber end at slightly different times. The modes of multimode fiber travel at different group velocities and therefore undergo different time delays, so that a short-duration pulse of multimode light is delayed by different amounts and therefore spreads in time.

2.3 Properties of optical fiber transmission

The most important properties that affect system performance of an optical fiber are fiber attenuation and dispersion.

2.3.1 Attenuation

Attenuation (or transmission loss) is the reduction in intensity of light beam (signal) with respect to the distance traveled through a transmission medium. Attenuation is the result of light absorption, scattering and bending losses. Attenuation is defined as the ratio of optical input power (P_i) to the optical output power (P_o) and is given as a unit of length

$$\text{Attenuation} = \left(\frac{10}{L}\right) \log_{10} \left(\frac{P_i}{P_o}\right), \tag{2.20}$$

where L is the fiber length. Attenuation is measured in decibels/unit length (dB/L).

Absorption

Absorption is one intrinsic effect that contributes to the attenuation of light in an optical fiber, it is defined as the portion of attenuation resulting from the conversion of optical power into another energy form, such as heat.

Three factors explain absorption in an optical fiber:

- The intrinsic of basic fiber material properties
- Imperfections in the atomic structure of the fiber material
- The extrinsic (presence of impurities) fiber-material properties

Scattering

Scattering is another intrinsic effect which contributes to the attenuation of light in an optical fiber. Scattering losses are caused by the interaction of light with density fluctuation within the fiber. Density changes are produced when an optical fibers are manufactured, because, during the manufacturation of an optical fibers, regions of lower and higher molecular areas, relative to the average density of the fiber, are created. Light traveling through the fiber interacts with the density area. Light is then partially scattered in all directions.

Rayleigh scattering is the main source of loss for fibers operating between 700 nm-1600 nm. Rayleigh scattering occurs when the size of the density fluctuation (fiber defect) is less than one tenth of the operating wavelength of light.

Bend losses

Bend loss is the propagation losses in an optical fiber (or waveguide) caused by bending [13, 14]. So bending the fiber also causes attenuation. The bending loss can be classified, depending on the bend radius of curvature, on two types of bends: microbend or macrobend loss.

Microbend losses are small microscopic bends of the fiber axis that occur mainly when a fiber is cabled and are caused by small discontinuities or imperfections in the fiber. External forces are also a source of microbends, because it deforms the cabled jacket surrounding the fiber but causes only a small bend in the fiber, also microbend loss increases attenuation because low-order modes become coupled with high-order modes that are naturally lossy.

Macrobend losses are bends having a large radius of curvature relative to the fiber diameter; macrobend losses are observed when a fiber bend radius of curvature is large compared to the fiber diameter.

2.3.2 Dispersion

Dispersion is the phenomenon in which the phase velocity of a wave depends on its frequency, or when the group velocity depends on the frequency [15]. There are three main sources of dispersion in optical fibers: *intermodal* dispersion, *material* dispersion, and *waveguide* dispersion. These types of dispersion lead to pulse spreading.

Intermodal dispersion

Intermodal dispersion or modal dispersion is the phenomenon that the group velocity of light propagating in a multimode fiber depends not only on the optical frequency, but also on the propagation mode involved. Intermodal dispersion causes the input light pulse to spread. The input light is made of a group of modes. As the modes propagate along the fiber, light energy distributed among the modes is delayed by different amounts. The pulse spreads because each mode propagates along the fiber at different speeds. Since modes travel in different directions, some modes travel longer distances. Modal dispersion occurs because each mode travels at different distance over the same time span, as shown in Figure (2.11)

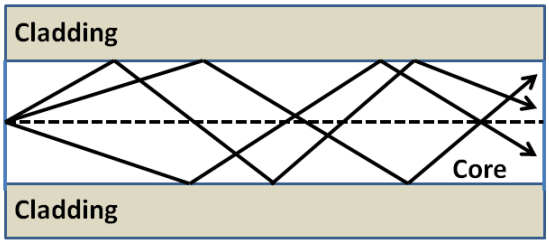

Figure 2.11. Distance traveled by each mode over the same time span.

The modes of light pulse that enter the fiber at one time exit the fiber at different times. This condition causes the light pulse to spread. As the length of the fiber increases, modal dispersion increases. Modal dispersion is the dominant source of dispersion in multimode fibers. Intermodal dispersion can be avoided by using single-mode fibers or can be diminished by using graded-index multimode fibers. Single mode fibers propagate only the fundamental mode. Therefore, single mode fibers exhibit the lowest amount of total

dispersion.

Material dispersion

Material (or chromatic) dispersion is due to the wavelength dependence of the refractive index. Optical fibers are made of glass which is a dispersive medium i.e., the refractive index is a function of wavelength. An optical pulse travels in a dispersive medium of refractive index n with a group velocity

$$v = \frac{c_0}{N} \tag{2.21}$$

where $N = n - \lambda_0 \frac{dn}{d\lambda_0}$ is called **group index**. Since the pulse is a wave packet each traveling at different group velocity, it width spreads. The temporal duration of an optical impulse of spectral width σ_λ (nm), after traveling a distance L through a dispersive material is given by [11, 15].

$$\sigma_\tau = \left| \left(\frac{d}{d\lambda_0} \right) \left(\frac{L}{v} \right) \right| \sigma_\lambda = \left| \frac{d}{d\lambda_0} \frac{LN}{c_0} \right| \sigma_\lambda \tag{2.22}$$

By recalling $N = n - \lambda_0 \frac{dn}{d\lambda_0}$, Equation (2.22) becomes

$$\sigma_\tau = \left| \frac{d}{d\lambda_0} \frac{1}{c_0} \left(n - \lambda_0 \frac{dn}{d\lambda_0} \right) \right| L\sigma_\lambda, \tag{2.23}$$

$$\sigma_\tau = \left| -\frac{\lambda_0}{c_0} \frac{d^2 n}{d\lambda_0^2} \right| L\sigma_\lambda, \tag{2.24}$$

which leads to a response time

$$\sigma_\tau = |D_\lambda| \, \sigma_\lambda L \quad \text{(Response Time)} \tag{2.25}$$

where D_λ is the material dispersion coefficient and it is defined as

$$D_\lambda = -\frac{\lambda_0}{c_0} \frac{d^2 n}{d\lambda_0^2} \tag{2.26}$$

The response time increases linearly with L, L is measured in km, σ_τ is ps, and σ_λ in nm, so that D_λ has units of ps/km-nm. This type of dispersion is called material dispersion. Material dispersion occurs because the spreading of light pulse is dependent on the wavelengths' interaction with the refractive index of the fiber core. The spectral width specifies

the range of wavelengths that can propagate in the fiber.

Waveguide dispersion

Waveguide dispersion is due to the dependence of propagation constant β which is a function of the size of the fiber's core relative to the wavelength of operation ($\mathbf{a}/\lambda_0$), when the index of refraction is assumed to be constant. Waveguide dispersion is particularly important in single mode fibers where modal dispersion is not present. The group velocity $v = \frac{d\omega}{d\beta}$ and the propagation constant β are governed by the fiber V-parameter

$$\mathrm{V} = \frac{2\pi\mathbf{a}}{\lambda_0}\mathrm{NA} = \frac{\mathbf{a}\mathrm{NA}}{c_0}\omega. \tag{2.27}$$

In the absence of material dispersion (i.e., when NA is independent of ω), V is directly proportional to ω, so that

$$\begin{aligned} \frac{1}{v} &= \frac{d\beta}{d\omega} = \frac{d\beta}{d\mathrm{V}}\frac{d\mathrm{V}}{d\omega} \\ \frac{1}{v} &= \frac{\mathbf{a}\mathrm{NA}}{c_0}\frac{d\beta}{d\mathrm{V}} \end{aligned} \tag{2.28}$$

The pulse broadening associated with a source of spectral width σ_τ is related to the time delay L/v by $\sigma_\tau = \left|\frac{d}{d\lambda_0}\frac{L}{v}\right|\sigma_\lambda$ [11]. Thus

$$\sigma_\tau = |D_\omega|\,\sigma_\lambda L, \tag{2.29}$$

where

$$D_\omega = \frac{d}{d\lambda_0}\left(\frac{1}{v}\right) = -\frac{\omega}{\lambda_0}\frac{d}{d\omega}\left(\frac{1}{v}\right) \tag{2.30}$$

is the waveguide dispersion coefficient. By substituting equation (2.27) into equation (2.30), one obtains

$$D_\omega = -\left(\frac{1}{2\pi c_0}\right)\mathrm{V}^2\frac{d^2\beta}{d\mathrm{V}^2}. \tag{2.31}$$

Thus the group velocity is inversely proportional to $\frac{d\beta}{d\mathrm{V}}$ and the waveguide dispersion coefficient constant is proportional to $\mathrm{V}^2\frac{d^2\beta}{d\mathrm{V}^2}$.

Chapter 3

Thulium Doped Fiber

3.1 Rare earth

The rare earth elements are a collection of twenty eight chemical elements in the periodic table, named the lanthanides and the actinides.

In this chapter, the electronic and optical properties of rare earth ions, the interaction between ions will be discussed. A special case of rare earth ion, thulium ion, will be investigated, the basic spectroscopy of the thulium ion will be also discussed.

3.1.1 Electronic and optical properties of rare earth ions

The rare earth elements are divided into two groups of 14 elements each, the lanthanides and the actinides. The lanthanides are characterized by the filling of the 4f shell, and the actinides by the filling of the 5f shell. For lasers and amplifiers only lanthanides are of great importance because many actinides have no isotopes stable enough to be useful for such devices [16]. In terms of optical and electronic properties, the most important feature of rare earth is the lanthanide contraction[1]. The lanthanide contraction is a consequence of imperfect screening by the 4f electrons, which leads to an increase in effective nuclear charge as the atomic number increases in the lanthanide series. The result of that imperfection is

[1]Decrease in ionic radii of the elements in the lanthanide series from atomic number 58, cerium to 71, lutetium, which results in smaller than otherwise expected ionic radii for the subsequent elements starting with 72, hafnium.

the 4f electrons become increasingly more tightly bound as Z increases [17].

In most cases, optical devises use trivalent (3+) ions because the trivalent level of ionization is the most stable for lanthanide ions. The ionization removes the 6s and 5d electrons, and the electronic configuration of the rare earth ions is that of the xenon structure , Z=54 ($1s^2 2s^2 p^6 3s^2 p^6 d^{10} 4s^2 p^6 d^{10} 5s^2 p^6$) plus $4f^N$ electrons, where $N = 1 - 14$. The optical spectra of trivalent rare earth ions observed is a consequence of transitions between 4f states. Since the 4f electrons interact only weakly with electrons on others ions, the Hamiltonian of the rare earth ions is given by:

$$H = H_{\text{free ion}} + V_{\text{ion-static lattice}} + V_{\text{ion-dynamic lattice}} + V_{\text{EM}} + V_{\text{ion-ion}}, \tag{3.1}$$

where $H_{\text{free ion}}$ is the Hamiltonian of the ion in complete isolation, $V_{\text{ion-static lattice}}$ and $V_{\text{ion-dynamic lattice}}$ contain the static and dynamic interactions of ion with the host material, V_{EM} deals with the interaction of the ion with the electromagnetic field, and $V_{\text{ion-ion}}$ treats the interaction between rare earth ions. The interaction terms in equation (3.1) are treated as perturbations because they are weak compared to the $H_{\text{free ion}}$, responsible for the observed electronic structure and dynamic, which induce transitions between the electronic states.

3.1.2 Electronic structure

Often Russel-Sanders coupling[2] (LS coupling) is used for the states of lanthanide and actinide, the states are labeled $^{2S+1}\text{L}_J$, where L, S, and J are the total orbital angular momentum, the total spin, and the total angular momentum, respectively. The total orbital angular momentum is specified by the letters S, P, D, F, G, H, I, K, ...for L= $0, 1, 2, 3, 4, 5, 6, 7, ...$, respectively. The angular dependency of the electrostatic interaction lifts the angular degeneracy and produces a spectrum of states the energies of which depend on L and S, not J. The spin-orbit lifts the degeneracy in total angular momentum and splits the LS terms into J levels. Figure (3.1) shows the energy diagram illustrating the hierarchy splitting resulting from electron-electron and electron host interactions [16].

[2]The total angular momentum L and the total spin angular momentum S of a multi-electron atom combined to form the total angular momentum J=L+S.

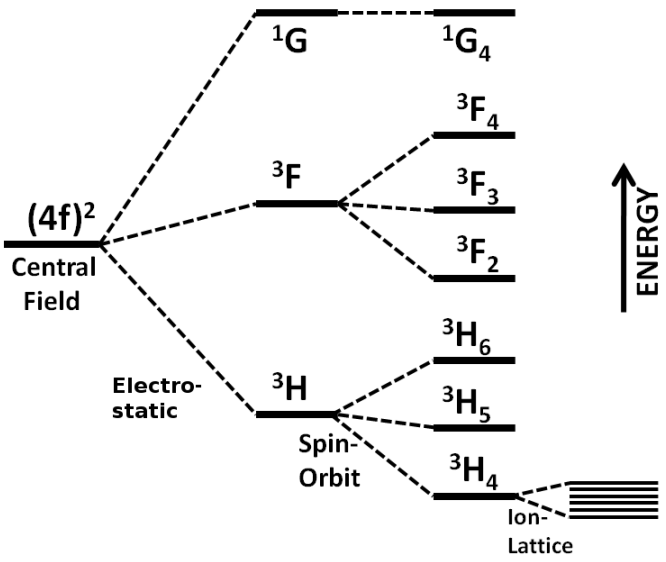

Figure 3.1. Energy diagram illustrating hierarchy of splittings resulting from electron-electron and electron host interactions.

3.1.3 Interactions between ions

The interaction occurring among rare earth ions can be accompanied with exchange of energy. This energy transfer can be beneficial or deleterious.

Energy transfer

The interaction between the rare earth ions is treated by $V_{\text{ion-ion}}$ in Equation (3.1). The most important manifestation of the $V_{\text{ion-ion}}$ is the transfer or sharing of energy between ions. The exchange or sharing of energy may occur among rare earth ions of the same or different species, and it may be either beneficial or deleterious. The techniques such as $Yb^{3+} \longrightarrow Er^{3+}$ energy transfer have been used to improve the pumping efficiency of devices of solid -state lasers, and $Er^{3+} \longrightarrow Er^{3+}$ energy transfer is a dissipative mechanism for fiber amplifiers at 1500 nm [18]. The phenomenon of radiative energy transfer involves one ion emitting a photon, which is then reabsorbed by another ion. The energy transfer is temperature dependent, because the ion-dynamic lattice interaction is involved. There are also some important processes involving excitation transfer between closely spaced ions without the exchange of real photons, such transfer of energy is called cross relaxation process.

Cross relaxation process

The cross relaxation energy transfer is a process in which an ion in an excited state transfers part of its excitation to a neighboring ion [5, 19, 20].

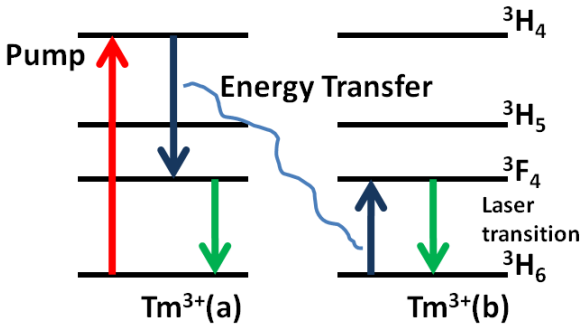

Figure 3.2. Cross relaxation process between two thulium ions

Figure (3.2) illustrates the cross relaxation energy transfer between two thulium ions. On this figure, the ion is excited into the $^3H_4$ level, the ion decays on the $^3F_4$ level, interacts with a nearby ion in the ground energy state. The first ion can transfer part of its energy to the second, leaving both in the $^3F_4$ level, both quickly decay non radiatively to the ground state. For the cross relaxation, the ions need not to be the same, and both may be in excited (but different) states. The cross relaxation process can be beneficial if one desires the ions to be in the excited states that result from the interaction.

Energy transfer up-conversion

The energy transfer up-conversion occurring in rare earth ions is believed to be the major cause of dissipation for some trivalent ion devices at 1500 nm [18]. The energy transfer up-conversion occurs when cross relaxation between an excited ion and one in the ground state cannot occur, the energy transfer up-conversion describes that if two excited ions interact, one can transfer its energy to the other, leaving itself in the ground state and the other in the higher state.

Figure (3.3) illustrates the phenomenon of energy transfer up-conversion, on figure (3.3a) both interacting ions are excited to the metastable $^4I_{13/2}$ level and on figure (3.3b) the

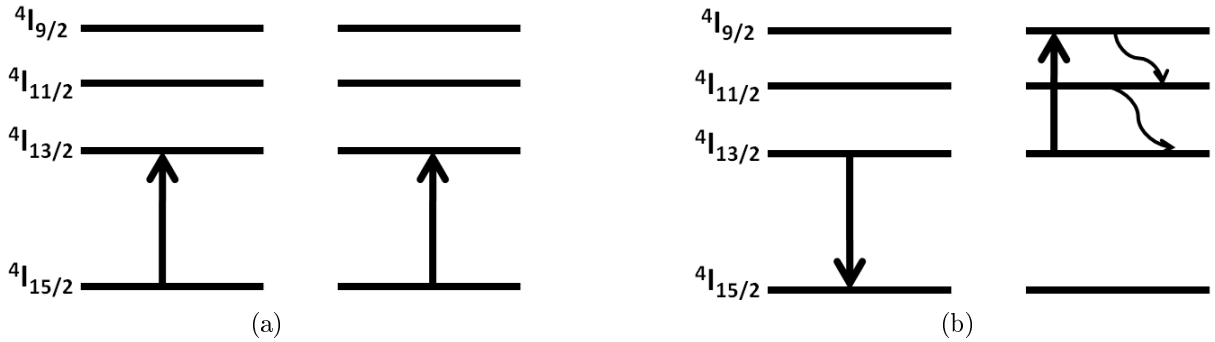

Figure 3.3. Illustration of energy transfer upconversion between two Nd^{3+} ions

donor ion transfer all its energy to the acceptor, leaving itself in the ground state and the acceptor in the $^4I_{9/2}$ state. For oxide glasses, the acceptor ion quickly decays non radiatively back to the $^4I_{13/2}$ level. The net result of the process is the conversion of one unit of excitation into heat.

3.2 Thulium ion

3.2.1 History and Uses

Thulium is a metallic chemical element in the lanthanide group on the periodic table of element. It belongs to the lanthanide series, which starts with lanthanum (La, Z=57) and ends with lutetium (Lu, Z=71). Thulium has an atomic number 69 and its atomic weight is 168.93421. Table (3.1) shows a specifications of the thulium on the periodical table. Thulium was discovered by a Swedish chemist, Per Theodor Cleve, in 1879 [21]. Cleve

Atomic Number	69
Atomic Weight	168.93421
Melting Point	1818 K (1545°C or 2813°F)
Boiling Point	2223 K (1950°C or 3542°F)
Density	9.321 g/cm^3 (room temperature)
Phase at room temperature	Solid
Element Classification	Metal

Table 3.1. Classification of thulium on the periodic table

uses the same method Carl Gustaf Mosander [21] used to discover lanthanum, erbium and terbium. He looked for impurities in the oxides of rare earth elements. He started with erbia, the oxide of erbium (Er_2O_3), and removed all the known contaminants. After further processing, he obtained two new materials, one brown and the other green. He named the brown material *holmia*, which is the oxide of holmium, and the green material *thulia*, which is the oxide of thulium. Nowadays, thulium is obtained through an ion exchange process from monozite sand ((Ce, La, Th, Nd, Y)PO_4), which is a material rich in rare earth elements that can contain as much as 0.007% thulium [22].

Thulium (Tm) plays an eminent role among numerous rare-earth dopant with its strong absorption lines at 785 nm and 685 nm [23] which are suitable for pumping by standard laser diodes, and has often been the preferred choice as an active ion for laser action in the infrared and upconversion to blue. While Nd^{3+} has been the most commonly used dopant ion in diode laser pumped solid-state lasers, Tm^{3+} is also of interest for obtaining different wavelengths and achieving high energy storage.

3.2.2 Basic spectroscopy

3.2.3 Energy level diagram of thulium

The electronic levels of thulium are $^3H_6$ (ground electronic level),$^3F_4$, $^3H_5$, $^3H_4$, $^3F_{2,3}$, $^1G_4$, and $^1D_2$. The energy level diagram of Tm^{3+} in silica is shown in Figure (3.4). The thulium element presents three major absorption bands in the infrared (IR), which are transitions $^3H_6 \longrightarrow {}^3F_4$ ($\sim$ 1630 nm),$^3H_6 \longrightarrow {}^3H_5$ ($\sim$ 1210 nm), and $^3H_6 \longrightarrow {}^3H_4$ ($\sim$ 790 nm).

3.2.4 Emission properties

The $^3F_4$ level is the main metastable level, relaxation of $^3F_4$ level is a non-radiative transition. The measured lifetime ranges from 200 μs to 300 μs [24, 25], 500 μs [24, 26], and 600 μs [27]. The lifetime is mostly non-radiative because of the high phonon energy of silica. In silica, the decay of the $^3H_4$ level to the $^3H_5$ level is non-radiative and its weakly metastable, the lifetime is $\leq$ 10 μs [25]. In most amplifiers, this level has been pumped directly at the 800 nm absorption band and this level is susceptible to cross relaxation process if the

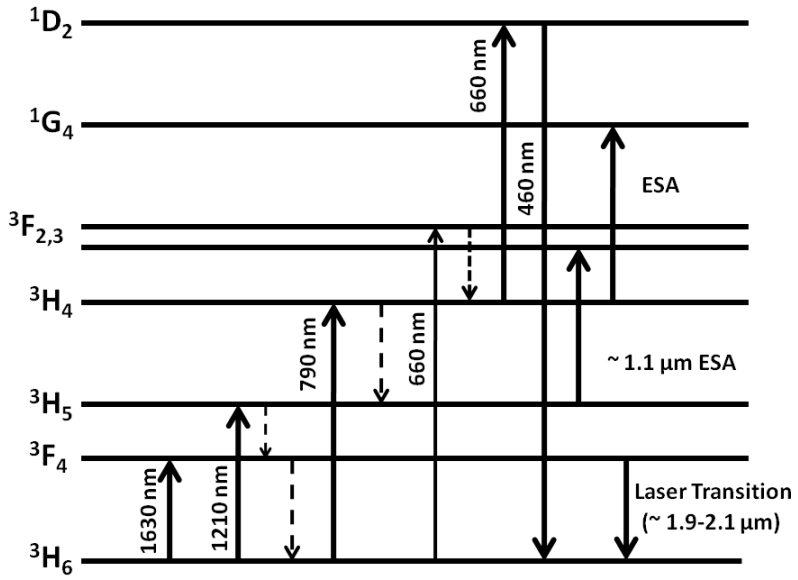

Figure 3.4. Energy level diagram of Tm^{3+} in silica. The solid lines are radiative transitions and the dashed lines are nonradiative transitions.

concentration is high. The $^3H_5$ level has a short lifetime because it is strongly coupled non-radiatively to the nearby $^3F_4$ level. The decay of the $^1G_4$ level to the ground state is completely radiative in fluoride glasses and largely radiative in silica with a quantum efficiency exceeding 50 %. The relaxation of the $^1D_2$ level is a radiative transition with short radiative lifetimes.

3.2.5 Laser transition

All Tm-doped silica fiber reported have been operated around 1.9 μm on the $^3F_4 \longrightarrow {}^3H_6$ transition. One of the most prominent advantages of thulium is the big bandwidth of the $^3F_4 \longrightarrow {}^3H_6$ transition and such bandwidth makes Tm-doped silica a great source of coherent radiation at mid-IR wavelengths which is not available from other rare-earths. This laser is quasi-three-level near 1.9 μm, four level-level at longer wavelengths. The wavelength of Tm-doped fiber lasers includes the strong absorption overtone of water around 1.98 μm, a wavelength used in a wide of micro-surgical procedures, such as laser angioplasty, blood coagulation, and microsurgery. This laser is also expected to find applications in eye-safe LIDAR (Light Detection And Ranging) and atmospheric sensing, in particular the detection of CO_2 and methane, which exhibit absorption lines in this range.

3.2.6 Pump wavelength

The $^3H_6 \longrightarrow {}^3F_4$ absorption band of Tm-doped silica possesses an extremely broad linewidth, close to 130 nm, it is one of the broadest in any of the trivalent rare earths [16]. The pump band mostly used is $^3H_6 \longrightarrow {}^3H_4$ transition at about 800 nm, which exhibits no significant excited-state absorption (ESA). The $^3H_6 \longrightarrow {}^3H_4$ transition is very broad, and it allows pumping at the strong peak near 790 nm with either AlGaAs laser diode or Sapphire laser. One important feature of this transition is the cross-relaxation between Tm^{3+} pairs, which takes place at higher Tm concentrations [28]. The cross-relaxation process leads to energy transfer from a Tm^{3+} ion in the $^3H_4$ level (donor) to a neighboring Tm^{3+} ion in the ground state (the acceptor). The latter is thus excited to the upper laser level ($^3F_4$ level), whereas the donor drops to the $^3F_4$ level, yielding two excited ions for one pump photon, or a quantum efficiency of 2 [5] as shown in Figure 3.1. The phenomenon of cross-relaxation has been used to pump a fiber laser with high Tm concentration [28].

3.3 Thulium-doped fiber lasers

Recent advances in fiber technology have produced demonstrations of high power fiber lasers that can generate output powers of several kilowatts. To date, the highest power devices have been based on ytterbium (Yb^{3+})-doped silica fibers that operate in the wavelength region centered around 1 μm. Lasers in this wavelength region are serious eye hazard since their beams are invisible but the power can be imaged onto the retina. At present, the power scaling of thulium-(Tm)-doped fiber lasers, emitting in the so-called "eye-safe" wavelength region around 2 μm, is investigated. Tm-doping is especially interesting for high power laser operation due to the possibility of cross relaxation process [6, 29], on which one can have 2 laser photons with one pump photon. The dependence of the threshold, slope efficiency, and laser wavelength can be adjusted by varying or changing the fiber length or the reflectivity of the mirrors [6, 30]. By varying these two parameters, one could adjust the laser wavelength from 1877 to 2033 nm.

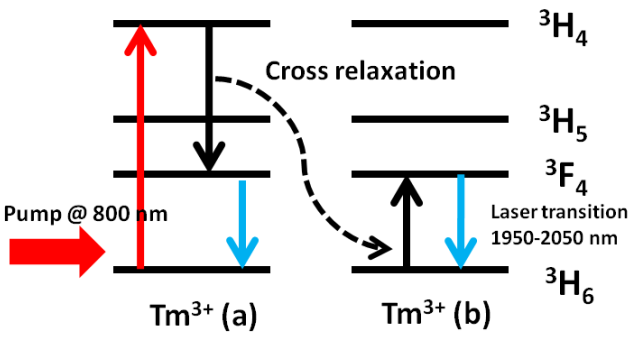

Figure 3.5. Cross Relaxation Energy Transfer between Two Thulium ions

3.3.1 High power lasers

A thulium-doped fiber laser near 2 μm is of great interest because of the possibility of combining high efficiency, high output power, and retina safety in addition to specific applications associated with this wavelength, such as remote sensing and biomedical applications [31]. Thulium exhibits a significant advantage over other rare-earth ions in that the slope efficiency can exceed the stokes limit [31] and a quantum efficiency near 2 can be achieved because of the cross relaxation energy transfer between thulium ions. The high doping concentration of thulium ions ensures cross-relaxation energy transfer by bringing the thulium ions closer.

Chapter 4

Experimental Setup

4.1 Setup for the characterization of Tm-doped fiber for mid infrared laser applications

The setup used for the characterization of the thulium doped fiber is shown in Figures (4.1) and (4.12). The diode laser is powered by a commercial Line Interactive UPS (Uninterrupted Power System) B2000, which supplies a maximum current of 10.8 A. The temperature of the diode is controlled by an OSTECH (Diode Laser Source DS×1 laser driver and temperature controller), which drive the laser and control the temperature of the diode laser. The output from the diode laser is collimated by a lens on an adjustable mount, connected to the diode laser by a fiber with 400μm diameter and an N.A. of 0.22. M_1 and M_2 are two dichroic mirrors coated for reflection at 800 nm and transmission at 2000 nm wavelength. M_1 and M_2 are placed in a such way they make an angle of 45°with an incident beam, so the reflected beam exits at a convenient angle of 90°. L_1 and L_2 are the collimated lens and the focus lens, respectively. The beam is focused into the Tm-doped fiber with L_1 and the feedback is made with a gold mirror M_3. The output of the laser occurs at M_2.

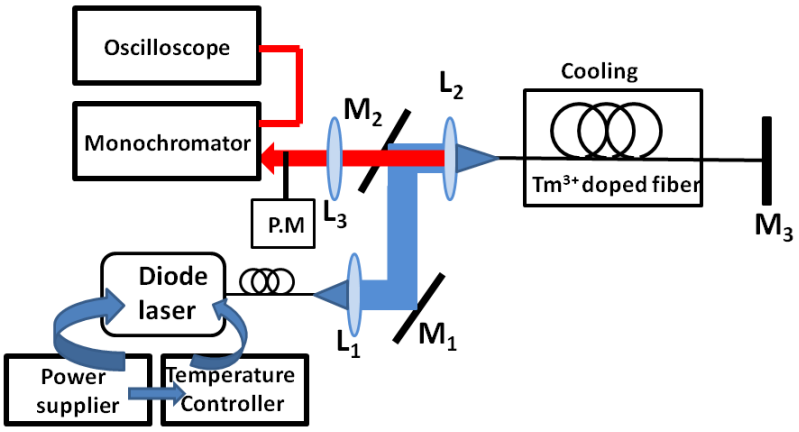

Figure 4.1. Setup of the Tm-doped fiber laser for mid infrared laser applications

4.2 Characterization of the diode laser

4.2.1 Specification

The diode laser (JOLD-75-CPXF-2P W) used, as shown in Figure 4.2, has a maximum output power of 75 W and operates with continuous wave (CW) output at a central wavelength of 808 nm at a temperature of 25°C. The operating current is 59 A, a threshold of 10 A and a typical slope efficiency of 1.6 W/A. The operating temperature of the diode laser ranges from 15°C to 30°C, measured with internal temperature sensor, according to the specification sheet [32]. The diode laser has a cooling system for which the water temperature ranges from 8°C to 23°C, with a flow rate of 3l/min. Cooling is done to just below room temperature, well above dew-point temperatures to avoid the formation of water droplets on the diode laser as a result of condensation. Cooling is advantageous over heating as the latter decreases the efficiency of the diode laser. The output power from the diode laser is connected to a free standing fiber inside F-SMA 905 towards the module. A pilot laser is incorporated in the diode laser, which has a maximum output power of 3 mW, for a central wavelength of 650 nm ± 10 nm, and maximum operating current of the pilot laser is 115 mA. The power of the pilot laser is not adjustable.

Figure 4.2. Diode laser used in the experimental setup [3]

4.2.2 Characterization of the diode

Experiments on the diode laser were conducted to determine the threshold and the slope efficiency of the diode laser, on the variation of the wavelength with respect to the current and temperature. Figure (4.3) shows the setup used for the characterization of the diode

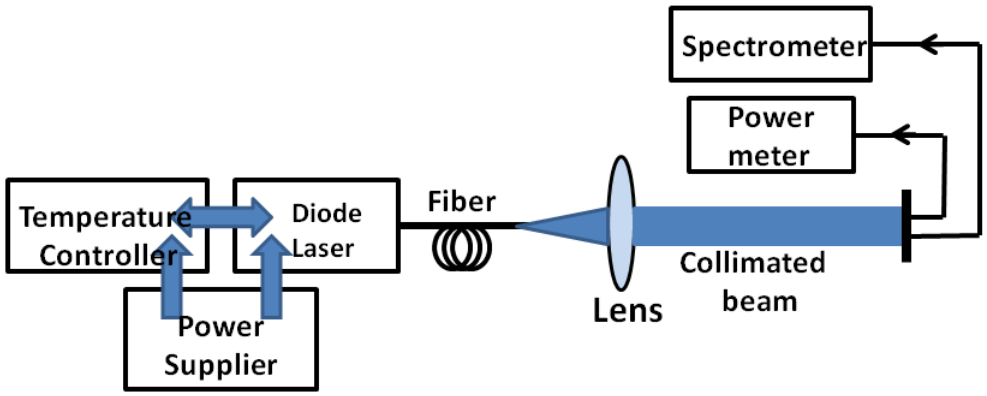

Figure 4.3. Schematic setup for the characterization of the diode laser

laser. The spectral intensity of the pump diode was recorded using Agilent Optical Spectrum Analyzer 86140 series. The output power of the diode laser was recorded using the Coherent Fieldmaster power meter, which was aligned at the collimated beam after the

lens. The electrical input power of the diode was measured by noting the current and the voltage from the OSTECH. The electrical input power is given by

$$P_{el} = \mathrm{V} \times \mathrm{I}, \tag{4.1}$$

where V and I are the voltage and the current, respectively.

4.3 Beam collimation

The laser beam coming out from the diode is divergent in the far-field. This suggests that the output beam cannot be used for any experimental work without proper collimation. The pilot laser (650 nm wavelength, 3 mW output power) was used for collimation. The diode delivery fiber and the lens L_1, with 15 mm focal length, are mounted together on a translation stage. The lens can be adjusted back and forward by means of a fine screws to achieve collimation. The collimated beam is reflected by M_1 and M_2, which are placed

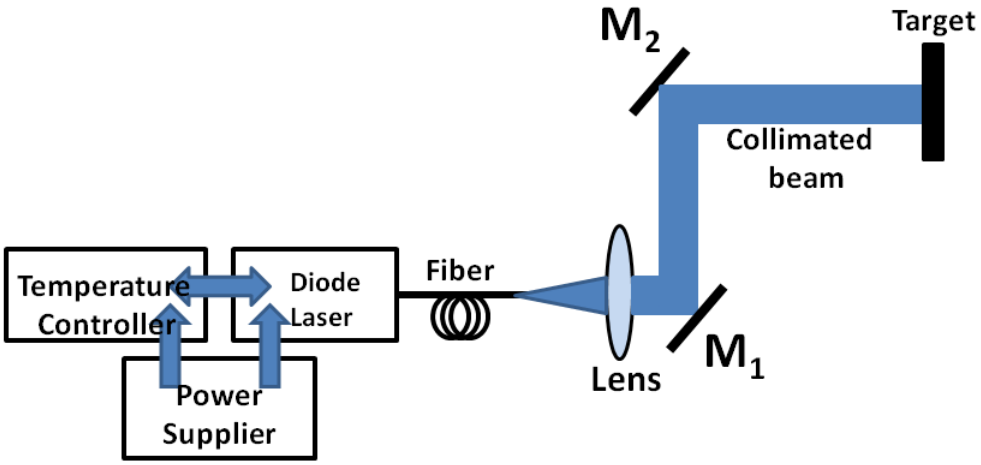

Figure 4.4. Setup used for the collimatiom of the beam

at approximately 45°of the incident beam. The collimated beam is imaged on a target to appreciate the good beam quality as shown in Figure 4.4.

4.4 Mirrors Characterization

The mirrors were characterized using the PERKIN ELMER Spectrometer, which has double-beam, double monochromator, ratio recording UV-Visible-Near Infrared Spectrometer with microcomputer electronics, video display, and soft keys operating system. The

Figure 4.5. Perkin Elmer Spectrometer [4]

Perkin Elmer, PE lambda 9 Spectrometer has a wavelength range from 185 nm to 3200 nm. The mirrors were placed inside the dual sample compartment, and the transmission of the mirrors recorded on the screen.

4.5 Fiber preparation

The thulium doped silica fiber used is manufactured by CorActive (Specialty Optical Fiber manufacturer) [33]. The fiber has a Tm^{3+} concentration of 5 wt%, and it is called triple-Clad Fiber (TCF) or Double-Clad Fiber (DCF) with two cores.

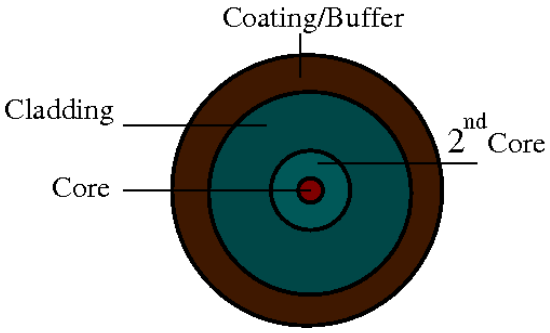

Figure 4.6. Triple Clad Fiber (TCF)

The specifications of the fiber is given by table (4.1) The preparation of the fiber involves

Specification	Data
Core diameter	18.1 μm
Second Core diameter	48.8 μm
Effective N.A.	0.11
Second Core Effective N.A.	0.23
Cladding diameter	403 μm
Second Cladding diameter	548 μm

Table 4.1. Fiber Specifications

two processes: cleaving process and polishing process.

4.5.1 Cleaving process

Fiber optics cleaving is the process to scribe and break an optical fiber end face. The goal of cleaving the fiber is to produce a mirror like fiber end face for fiber splicing, for fusion splicing or mechanical splicing. In order to make a good fiber splicing or to couple light inside the fiber, good cleaving is required. Usually bad cleaving has to be redone.

Tools needed:

∗ Fiber stripping

∗ Fiber

∗ Alcohol

∗ Cleanex

∗ Eye loupe or microscope

∗ Cleaver

Procedure:

⋆ Use the stripper to remove the jacket/ buffet from one end of the fiber

⋆ Clean bare fiber using alcohol

⋆ Prepare the cleaver, ensure that tension level is horizontal and blade release lever up

⋆ Place the fiber in the grooves

⋆ Gently lower clamps to hold fiber

⋆ lock left hand clamp down

⋆ Then lock right hand clamp down

⋆ Move tensioning lever down

⋆ Move blade release lever down

⋆ Remove cleaved fiber and cutoff

Make sure the cleaved fiber does not touch anything.

4.5.2 Polishing process

Polishing the fiber is part of the cleaving process. Polishing the fiber is the process to make a cleaved fiber clean and smoothly shaped and leads to the highest surface quality and angular accuracy.

Tools needed:

∗ Polishing plate

∗ Flexible rubber pad

∗ Polishing disc

∗ Connector

∗ Alcohol

∗ Lint-free towel moistened

(a) Rubber pad+connector+microscope (b) Polishing films

Figure 4.7. Polishing Tools

∗ Eye loupe or microscope

∗ polishing films (5μm, 3μm, 1μm, 0.3μm)

Procedure:

⋆ Clean the surface of the glass plate and the rubber pad with a lint-free towel moistened with isopropyl alcohol

⋆ Clean the polishing disc and connector

⋆ insert the connector into the polishing disc

⋆ Place the fiber polishing film on the rubber polishing pad

⋆ Start polishing the fiber with the 5μm polishing film by making a figure of 8 pattern. Figure 4.7 shows some of the cleaving and polishing tools used.

⋆ Replace the 5μm polishing film with 3μm polishing film, and so on

⋆ Remove the connector from the polishing disc and clean the connector with isopropyl alcohol

⋆ Using a 100X inspection microscope, ensure that there are no heavy scratches through the core of the fiber. Light random scratches in the fiber cladding are acceptable. However,

the majority of the area of the fiber should be free of all visible scratches or defects.

4.6 Coupling light into the fiber

The ability to couple light from free space to fiber and collimate the fiber output is crucial. The optical power that can be coupled into a fiber depends both on the parameters of the fiber (numerical aperture and core diameter) as well as on the brightness of the used optical source. To couple a light beam with a diameter D_i and wavelength λ into the fiber with numerical aperture NA and mode field diameter **a**, one has to use a lens (focal length f) and focus the beam to a diameter (D_f) approaching the mode field diameter of the fiber **a**

$$D_f = \frac{4\lambda f}{\pi D_i} \leq \mathbf{a} \tag{4.2}$$

D_f is the diffraction limited spot size, i.e. the best or smallest spot one can achieve with the system with perfect focus and perfect optics.

On the other hand, the divergence of the focused beam, should not exceed the numerical aperture (NA) of the fiber ($\mathrm{NA}_{lens} \leq \mathrm{NA}_{fiber}$), which leads to the condition

$$f \geq \frac{D_i}{2NA} \tag{4.3}$$

The setup used to couple light into the fiber is given by Figure (4.8). The power coming out of the diode laser, after the focus lens, serves as reference.

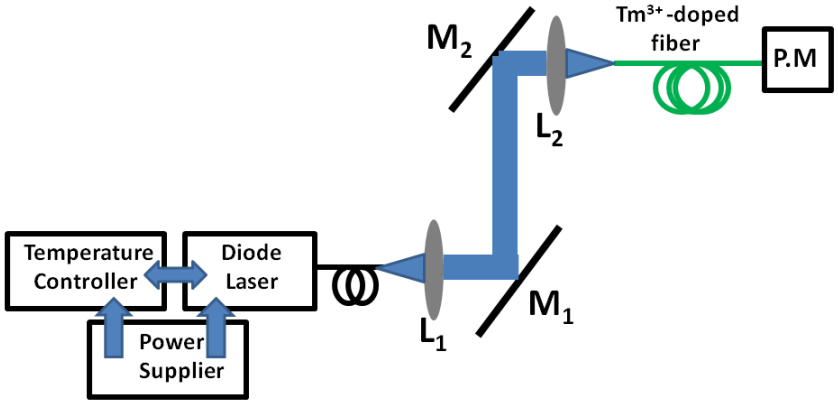

Figure 4.8. Setup used to couple light into the fiber

For good coupling, the beam needs to hit the center of the focus lens, and it is focused into the fiber in such a way that the incident angle must be less than the acceptance angle (equation 2.5), so it can propagates inside the fiber by total internal reflection. The power meter (P.M.) is placed at the end of the fiber to measure the amount of power that was getting coupled.

4.6.1 Choice of lenses

Assuming that D_{f_1} and D_{f_2} are the diffraction limited spot size, with numerical aperture NA_1 and NA_2, respectively. Using equation (4.2) and inequation (4.3), one can show

$$D_{f_2} = \frac{f_2}{f_1} D_{f_1}, \tag{4.4}$$

where f_1 and f_2 are the focal lengths of the collimated lens and the focus lens, respectively. In the experiment $f_1 = 15$mm, $f_2 = 8$ mm and $D_{f_1} = 400$ μm. Thus the spot diffraction limited spot size on the fiber is $D_{f_2} = 213.33$ μm ≤ 400 μm (cladding diameter of the fiber). With the value of D_{f_2} obtained, all the beam is focused in the fiber with 400 μm diameter.

4.7 Diffraction grating

4.7.1 Choice of the grating monochromator

The purpose of the use of the grating monochromator was to determine the central wavelength of the output of the Tm-doped fiber laser.

The monochromator used to characterize is the Jarrell-Ash 0.5 Meter Ebert Scanning Spectrometer, Model 82-001. The spectrometer provides excellent optical performance in a compact, rugged, reliable instrument with both motorized and manual drive. The instrument assures excellent definition to enable the utilization of high resolving power of different diffraction gratings. The motor and the reduction gear system provide a smooth scanning motion in eight speeds, ranging from 2 A/min to 500 A/min, with a counter

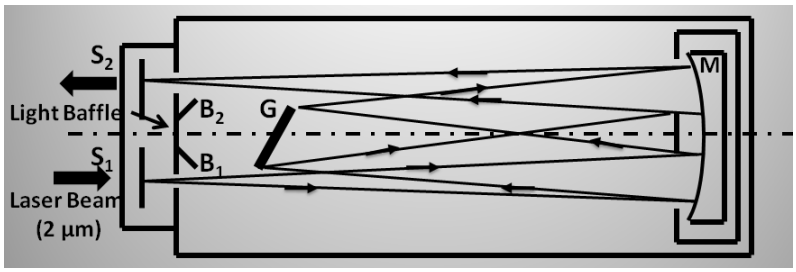

Figure 4.9. Optical Diagram of Ebert Scanning Spectrometer

reading directly in angstrom units, based on 1180 groove/mm grating.

The optical diagram of the Ebert monochromator used for the determination of the central wavelength of the Tm-doped fiber laser is shown on Figure (4.9). Table (4.2) shows the optical specification of the half meter Ebert Scanning Spectrometer [34].

Focal length	0.5 meter
Grating	Plane reflection, blazed for 2μm 300 g/mm
Mirror	150 mm diameter, concave 0.5 m focal length
Effective Aperture ratio	f/8.6
Reciprocal Linear Dispersion	64 A/mm (295 groove/mm grating) in first order

Table 4.2. Optical Specifications of the Jarrell-Ash 0.5 Meter Ebert Scanning Spectrometer, Model 82-001

4.7.2 Description of the optical system

Laser beam enters slit S_1 and passes to the 150 mm diameter concave mirror M where it is collimated and reflected as parallel beam to a plane grating G. The dispersed beam is reflected back to the mirror M where it is again reflected and focused on the exit slit S_2 (see Figure 4.9). The central wavelength of the laser beam emerging at the exit slit is obtained by simply rotating the grating about its center.

4.7.3 Grating equation

The grating is an optical component with a periodic structure, which splits and diffracts light into several beams traveling in different directions. The directions of the different beams depend on the spacing of the grooves and the wavelength of the incident light on the grating surface [35]. Figure (4.10) shows the schematic diagram of a parallel rays of

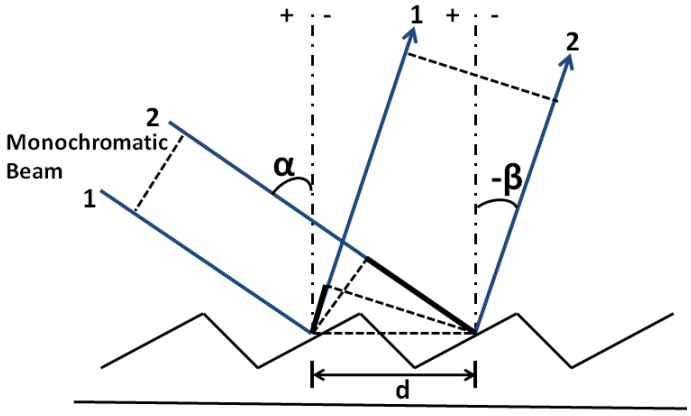

Figure 4.10. Monochromatic beam incident on (blazed) diffraction grating at angle α and diffracted at angle -β. The blazed spacing is d.

a monochromatic radiation, from a single beam in the form of rays 1 and 2, are incident on a (blazed) diffraction grating at an angle α relative to the grating normal (which is normal to the grating surface, not necessarily to the grooves). The rays are then diffracted at an angle -β where constructive interference occurs. The negative sign is based on the convention that positive angles are measured to the left of the grating normal, and negative angles to the right. From Figure (4.10), ray 2 travels a greater distance than ray 1. The change in path lengths from beams 1 and 2 is given by

$$\Delta_1 = d \sin \alpha \tag{4.5}$$

and

$$\Delta_2 = d \sin(-\beta) = -d \sin \beta, \tag{4.6}$$

as illustrated on Figure (4.11), and where d is the groove spacing. The path difference $\Delta = \Delta_1 - \Delta_2$, which is an integer multiple m of wavelength λ, i.e. $\Delta = m\lambda$ [36], for

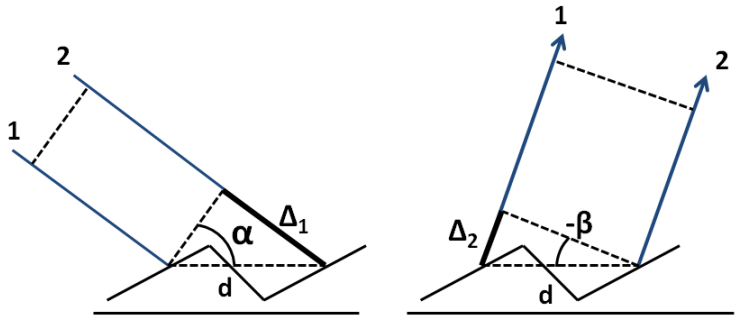

Figure 4.11. Illustration of path difference between incident and diffracted rays.

constructive interference. One can obtain the grating equation given by

$$\Delta = m\lambda = d\left(\sin\alpha + \sin\beta\right), \quad \text{for constructive interference} \tag{4.7}$$

where $m = 0, \pm1, \pm2, ..., k$, where k is a smaller integer and m the diffraction order. Equation (4.7) is the general grating equation using the positive/negative angle conventions.

The grating equation is sometimes defined as

$$m\lambda = d\left(\sin\alpha \pm \sin\beta\right), \tag{4.8}$$

where one uses the "subtraction" operation when α and β are opposite sides of the grating normal. In most of cases, the incident illumination is perpendicular to the grating surface, that means the incident angle $\alpha = 0$. In this case the grating equation (4.7) reduces to

$$m\lambda = d\sin\beta, \tag{4.9}$$

and when the incident light is diffracted back toward the direction from which it came, i.e. $\alpha = \beta$, the grating equation (4.7) becomes

$$m\lambda = 2d\sin\alpha, \tag{4.10}$$

which is called the Littrow configuration.

4.7.4 Calibration of the spectrometer

The calibration of the half meter Ebert Spectrometer was made using the Helium-Neon (He-Ne) laser operating at a wavelength of 632.4 nm (with a maximum output power of 15 mW) in the red part of the visible spectrum. The He-Ne was aligned with the spectrometer, and the laser light (from the He-Ne laser) was sent through the entrance slit of the spectrometer, the light was diffracted by the grating blazed at 2 μm (with 300 groove/mm). The diffraction patterns was observed at the exit slit of the spectrometer by rotating the grating. The spectrometer has four digit mechanical counters which provide direct wavelength readings in angstroms with a properly calibrated drive, when using an 1180 groove/mm grating. When using a 300 groove/mm, the wavelength reading should be multiplied by 4, according to the spectrometer's manual. High diffraction orders of the He-Ne laser were used to get multiple calibrations points. The spectrometer resolution is 0.8 Å in the first order for 300 groove/mm grating.

4.8 Measurement of the spectral output

The spectral output of the thulium doped fiber laser was recorded using an oscilloscope, connected to a DET10D photo detector [37]. The specifications of the InGaAs photo detector used to measure the spectrum is given in Table (4.3).

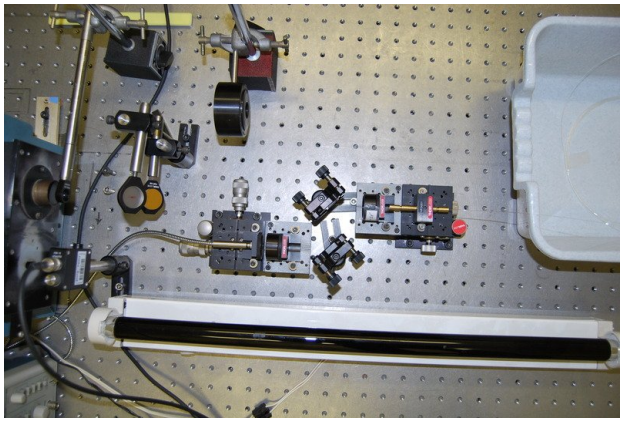

Figure 4.12. Top view of the Tm^{3+}-doped fiber laser setup.

Table 4.3. Specifications of the DET10D photo detector used to measure the Thulium doped fiber laser spectrum

Electrical		
Detector:		InGaAs PIN
Active Area:		0.8mm^2 (ø1mm)
Wavelength Range:	λ	1.2 to 2.6 μm
Peak Wavelength:	λ_p	2.3 μm
Peak Response:	$\Re(\lambda_p)$	1.1 A/W (typ)
Shunt Resistance:	R_{sh}	3kΩ@25°C (1kΩ@40°C)
Diode Capacitance:	C_J	175pF
Rise/Fall Time:	t_r	25ns (max.)
Linearty Limit:		1mW (min @ λ_p)
NEP (λ_p):		2×10^{-12} W/$\sqrt{\text{Hz}}$ (max.)
Detectivity (λ_p):	D*	$5{\times}10^{10}$ cm.W/$\sqrt{\text{Hz}}$
Bias Voltage:	V_{BIAS}	1.8V (Regulated)
Dark Current[2]:	I_D	15μA (75μA max.)
Output Voltage:	V_{OUT}	0 to 1.8V
Damage Threshold:		100mW/cm^2

4.9 Efficiencies and spectra measurements

The experimental setups used for the measurement of the efficiencies and spectra of the thulium-doped fiber, with different temperatures and different resonators are shown in Figures (4.1), (4.13), and (4.14). In Figure (4.1), the resonator is made of a high reflective

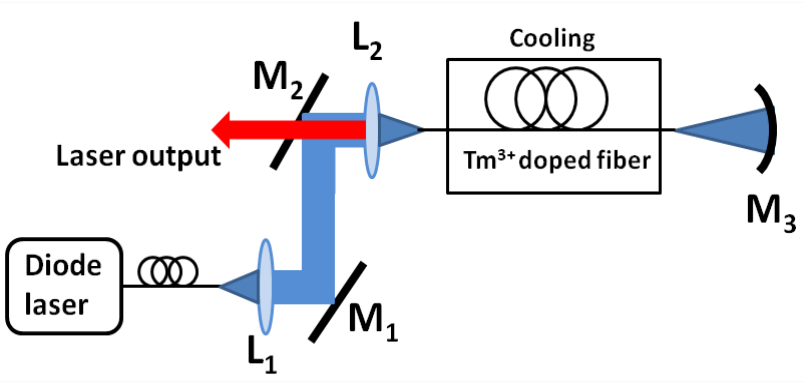

Figure 4.13. Schematic diagram of the experimental setup used for the characterization of the Tm^{3+}-doped fiber using a spherical mirror for back oscillations.

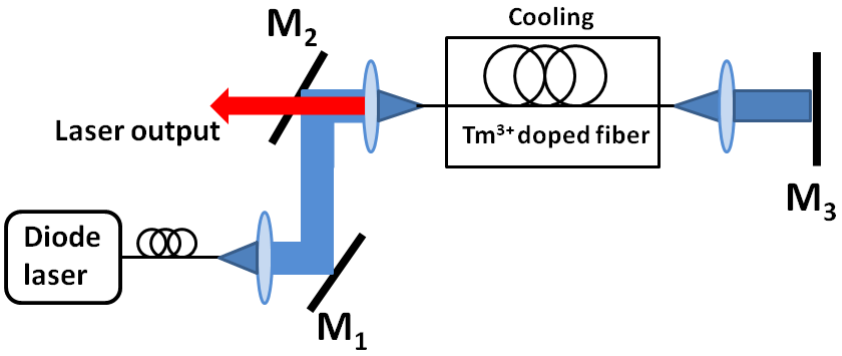

Figure 4.14. Schematic diagram of the experimental setup used for the characterization of the Tm^{3+}-doped fiber using a lens and a flat mirror for back oscillations.

mirror, placed in direct contact with the end fiber, and the fiber-air interface, which serves as a partially reflective mirror. The resonator in Figure (4.13) is made of a spherical mirror, for feedback oscillations, and the fiber-air interface, and the feedback oscillations is provided by a flat plane mirror in Figure (4.14). In all the resonator configurations, the pump light is collimated using a lens with 15 mm focal length, the light is reflected by the two dichroic mirrors (HR@800 nm, HT@2 μm), and then the collimated beam is coupled into the thulium doped fiber, where 90% of the pump beam is absorbed and 10% is transmitted to start the population inversion inside the fiber and amplification of the signal. The laser output is transmitted through the second mirror (M_2). The output power is measured using a power meter (Coherent Field master), the laser output is then aligned and collimated inside the diffracted grating spectrometer, and the spectral output is measured using a sensitive detector (DET10D photo detector), which is connected to an oscilloscope.

The characterization of the Tm^{3+}-doped fiber as an active medium was done in room temperature (25°C), by cooling the fiber with ice water (0°C), and -15°C, and using two prototypes of fiber: the first, with an active medium of 4 m doped with thulium ions and the second with 4 m of active medium spliced at both ends with un-doped fiber. The temperature of -15°C was achieved by mixing ice glasses with normal salt. The advantages of the two un-doped fibers spliced on the ends of the doped fiber are:

• the doped fiber can easily be maintained in the cooled compartment, and

• to eliminate the burning problems, observed with the Tm^{3+}-doped fiber without ends spliced with un-doped fiber, when the light was coupled into the fiber.

Chapter 5

Results and discussion

The experimental results obtained during this study and their discussions and analysis are presented in this chapter. Firstly, results obtained from the characterization of the diode laser are discussed in Section 5.1. Results of the characterization of the mirrors used in the experimental setup are discussed in Section 5.2. Results on the coupling efficiency and the characterization of the thulium doped fiber are discussed in Sections 5.3 and 5.4, respectively. The results of the Tm^{3+}-doped fiber efficiencies and spectra, at different temperatures, are presented and discussed in Section 5.5.

5.1 Characterization of the diode laser

The aim was to look for the threshold and slope efficiency of the laser, to investigate how the wavelength and power output of the diode laser varies with temperature and current in the absence of external optical feedback and to record the spectral intensity in terms of wavelength. The setup of Figure (4.3) was used to make a measurements on the efficiency and spectral intensity of the diode.

5.1.1 Diode efficiencies

The threshold is an operation condition of a laser when laser emission just starts to occur [38]. Below threshold, there is no sufficient population inversion to compete with

non-radiative recombination processes due to low pumping levels, therefore spontaneous emission dominates, to produce incoherent light. Above threshold, the increase in injection current causes an increase of optical output power as a consequence of gaining saturation. In this region the optical output power increases linearly with injection current as stimulated emission is increased into the active region of the diode laser.

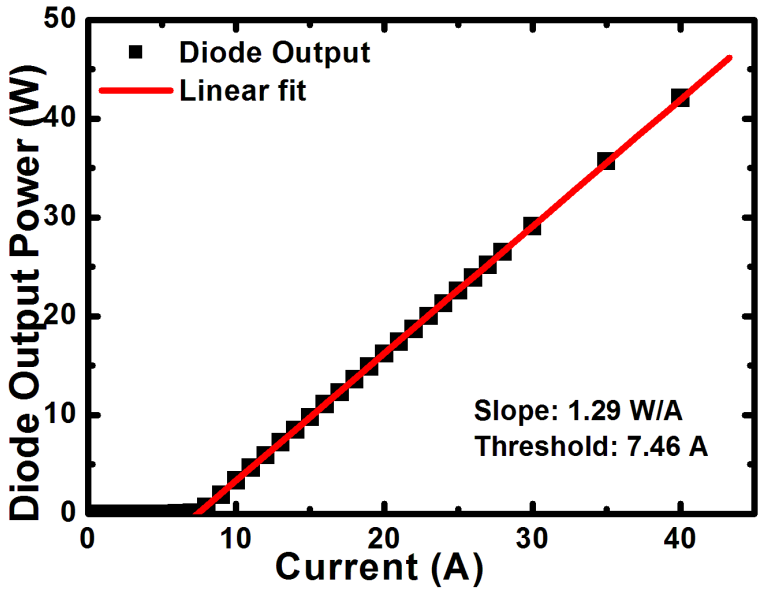

Figure 5.1. Efficiency of the diode laser

The optical output power was measured with a Coherent FieldMaster power meter at different injection currents from the diode. The results indicating the laser output vs current is shown in Figure (5.1). Figure 5.1 shows that at low injection currents the optical output power increases very little until the threshold I_{th} is reached at

$$I_{th} = 7.49\text{A}$$

The gradient of the line above threshold gives the slope efficiency of the diode laser, which is

$$\text{Slope efficiency} = 1.29\text{W/A}$$

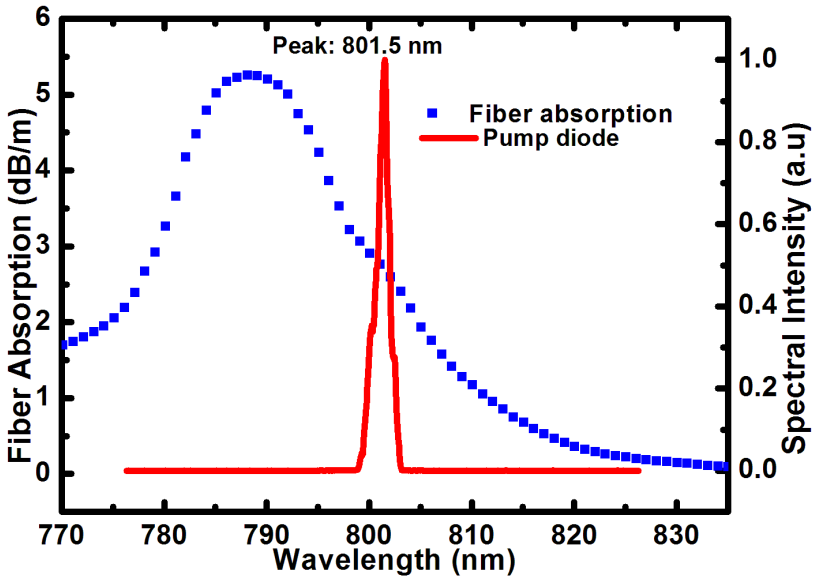

Figure 5.2. Spectral intensity of the diode laser and thulium absorption spectrum

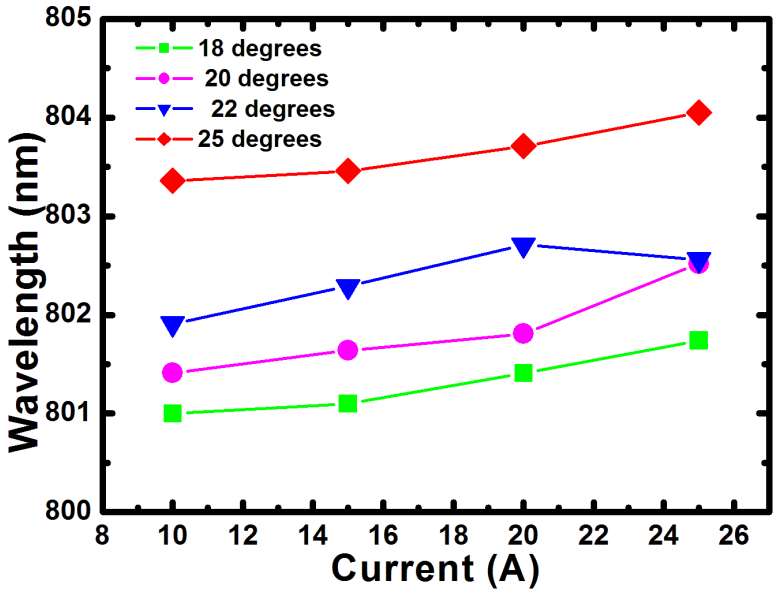

Figure 5.3. Variation of wavelength with output power for different temperatures.

The light intensity of the diode laser was measured using an optical spectrum analyzer [1]. The spectral intensity data was recorded and Figure 5.2 shows the data of the spectral intensity and the fiber absorption [33] characteristics on one graph. From the graph, it can be deduced that the diode laser emits the highest intensity (peak) at 801.509 nm with the

[1] Agilent 86140 Series

full width at the half maximum (FWHM) of 1.25 nm (not shown on the graph). The light intensity of the diode laser was measured for different injection current levels (10 A, 15 A, 20 A, 25 A) at different temperatures (18°C, 20°C, 22°C, 25°C). Figure 5.3 shows how the wavelength shifts with the current for different temperatures. From this graph, it can also be deduced that on average, for temperature between 18°C and 22°C, the wavelength shifts approximately about 0.25 nm/°C for a given current. From the graph shown in Figure (5.2), it can be seen that at the peak intensity, the absorption of the pump light by the thulium doped fiber is about 2.8 dB/m and also from Figure (5.2), it is clear that a small shift of temperature will still be in the absorption range of the fiber.

5.2 Mirrors characterization

The characterization of the dichroic mirrors was done by using the PERKIN ELMER Spectrophotometer. The transmission of the mirrors, in the wavelength range of [700 nm-2250 nm], was recorded; and the plots of the transmission of the mirrors is given by Figure (5.4). From the graphs, it is evident that all the dichroic mirrors are highly reflective

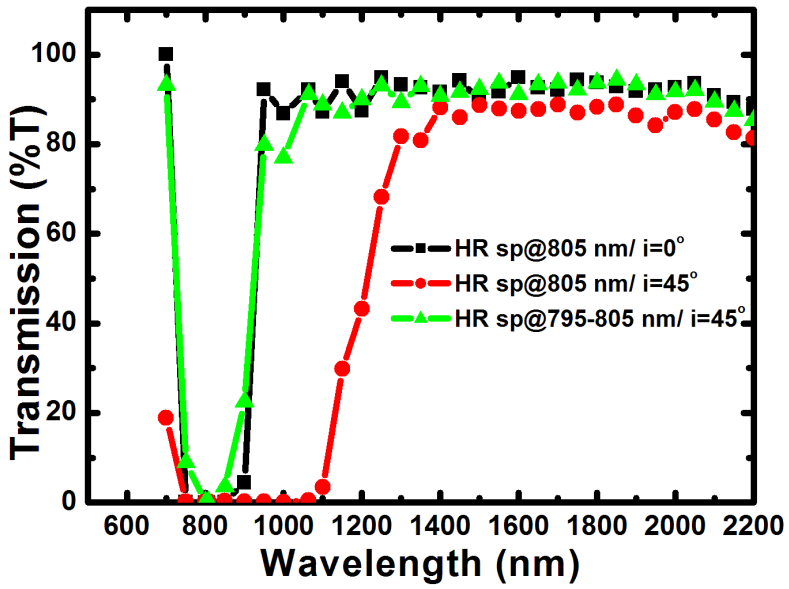

Figure 5.4. Mirrors transmission vs. wavelength

at 800 nm (input wavelength) and the dichroic mirror HR_{sp}@(795-815) nm/ i= 45°and HR_{sp}@805 nm/ i= 0°are highly transmissive at 2000 nm. For the purpose of the experiment

HR_{sp}@(795-815) nm/ i= 45°, with 90 % transmission at 2000 nm, was chosen as the output coupler of the thulium doped fiber laser because it offers the highest transmission of all tested mirrors at 2000 nm.

5.3 Coupling efficiency

The coupling efficiency was determined using the following steps: the diode laser was coupled into the fiber and the transmission was measured. By adjusting the coupling and optimizing the transmission, the coupling efficiency of the fiber was determined. The coupling efficiency of the light into the fiber was determined by using a short length of fiber (30 cm), and the pilot laser wavelength of 650 nm to avoid significant absorption inside the fiber. Hence the % transmission was a direct measure of the coupling efficiency. Table 5.1 summarizes the data of a best coupling efficiencies obtained after two alignments.

	Power after lens (μW)	Output end fiber (μW)	Coupling efficiency (%)
Alignment 1	288	257	82
Alignment 2	260	220	85

Table 5.1. Coupling efficiency

Alignment 2 was done with the collimating lens of 15 mm and the focus lens of 8 mm; this after a careful cleaving and polishing processes as shown in Figure (5.5). From these two pictures, a bad cleaving of the fiber generates damages and scratches on top of the fiber as shown in Figure 5.5a. Picture 5.5b shows a fiber after a polishing process. Without the polishing process, the input coupling efficiency drops to about $50-60\%$ due to scattering on the fiber end facet.

5.4 Characterization of triple-clad thulium doped fiber

The thulium doped fiber used was manufactured by a Canadian company (CorActive), which is specialized in producing fibers. The fiber has the specifications listed in Table

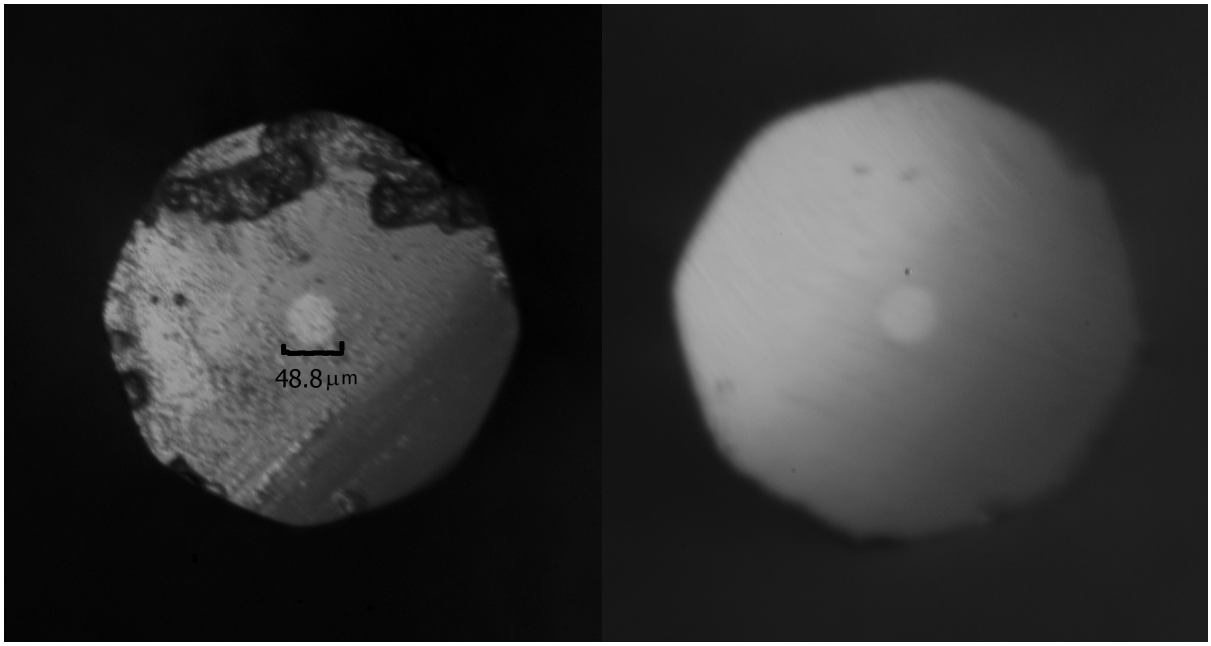

(a) Cleaved fiber (b) Polished fiber

Figure 5.5. Polishing the fiber

(4.1), a Tm^{+3} concentration of 5 wt%, and the fiber length used for the experiment is 4 m. The fiber length was optimized at 4 m because the goal was to get 90 % absorption of the pump light to achieve a population inversion over the fiber length. The thulium absorption around 800 nm is 2.7 dB/m (see Figure 5.6). To get 10 % transmission and 90 % absorption of the pump light around 800 nm, the optimum fiber length is $\frac{10m}{2.7} = 3.7$ m.

5.5 Calibration of the spectrometer

The He-Ne laser which was used for the calibration of the Ebert Half Meter Spectrometer emits at 632.8 nm. The wavelength display on the spectrometer is optimized for visible wavelengths using a 1180 groove/mm grating. Since we used a 300 groove/mm grating to extend the range of the spectrometer further towards the infrared, we used the higher diffraction orders of the He-Ne laser for the calibration. The spectrometer was calibrated in such a way that the fourth order of the diffracted beam on the grating corresponds to 632.8 nm on the wavelength display. In the subsequent measurements, the reading on the spectrometer was then multiplied by a factor of 4 to yield the true wavelength value.

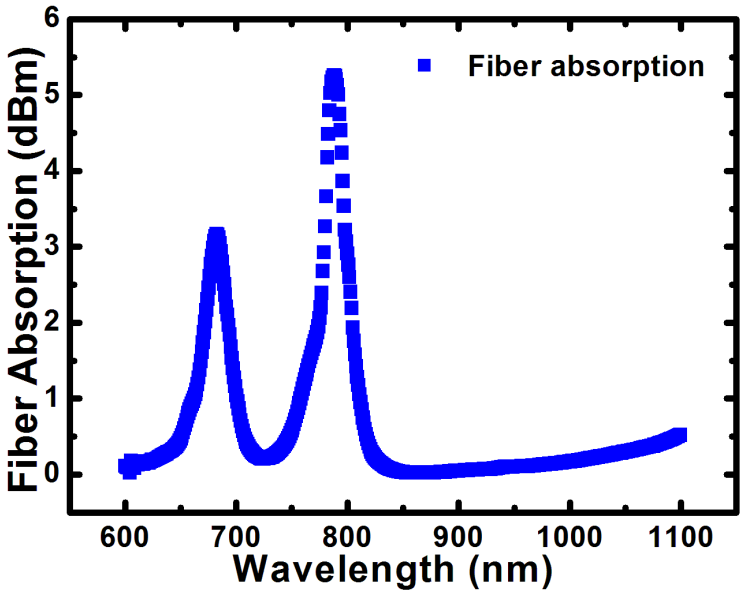

Figure 5.6. Spectrum of the absorption of the Tm^{+3} from 600 nm to 1100 nm

The diffraction orders of the He-Ne laser and the wavelength readings on the spectrometer are shown in Table (5.2), and the calibration curve (error), function of the true values

Diffraction Order	Second Order	Third Order	Fourth Order	Fifth Order
True values (nm)	316.4	474.75	632.8	791.25
Readings (nm)	314.8	474.2	632.8	790.3

Table 5.2. Diffraction orders of He-Ne laser and wavelength readings on the spectrometer

is displayed in Figure (5.7). The result on the wavelength calibration shows that the wavelength reading error for the spectrometer is approximately ±1.6 nm.

5.5.1 Efficiencies and spectrum of the bare Tm^{3+}-doped fiber without un-doped pieces.

In this section, slope efficiency and the spectrum of the Tm^{3+}-doped fiber is measured, for the fiber without un-doped fibers spliced at the end doped fiber. The measurements were conducted with fiber in ambient air and secondly the thulium doped fiber was cooled with

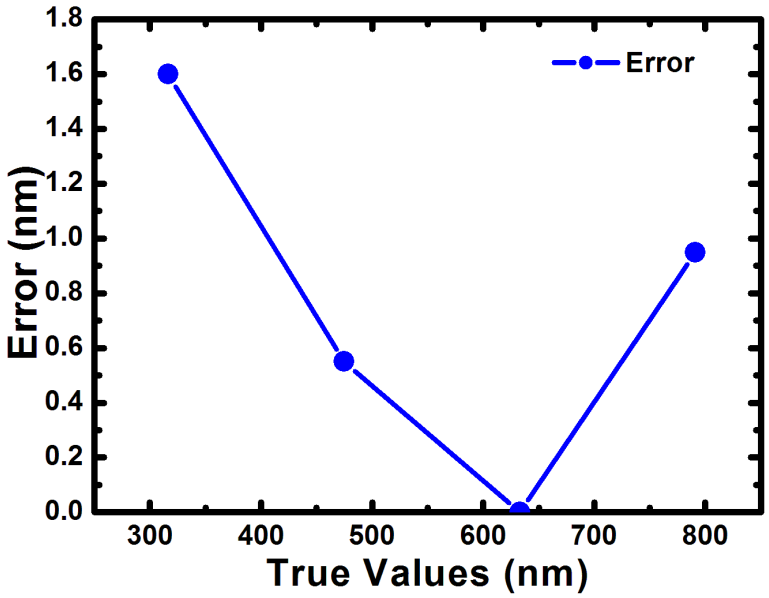

Figure 5.7. Calibration curve of the spectrometer

ice water (≈ 0°C). In ambient air, the laser output power was not stable; the output power decreased with time due to thermal effects. Pumping the fiber at 800 nm, data collected after the focusing lens (see Figure 4.1) and the laser output power are given by Table (5.3)

The Absorbed Power is defined as

$$\text{Absorbed Power} = 0.85 \times 0.9 \times (\text{Power After Lens}), \tag{5.1}$$

where 0.85 is the value of the coupling efficiency and 0.9 the fraction of injected light which is absorbed in the fiber; and Real Output is the fiber output, and it is defined as

$$\text{Real Output} = 1.389 \times (\text{Output}), \tag{5.2}$$

where the factor of 1.389 accounts for the losses at the collimating lens (20 %) and the 45°mirror (10 %) at the output of the laser.

If X is the fiber output power and Y the laser output, then

$$\mathrm{X} - \frac{20}{100}\mathrm{X} - \frac{10}{100}\left(\frac{80}{100}\mathrm{X}\right) = \mathrm{Y} \tag{5.3}$$

Current (A)	Power After Lens (W)	Output (W)	Absorbed Power (W)	Real Output (W)
20	12.1	0.17	9.2565	0.23613
21	13.1	0.40	10.0215	0.5556
22	14.2	0.67	10.863	0.93063
23	15.1	0.93	11.5515	1.29177
24	16.2	1.19	12.393	1.65294
25	17.1	1.46	13.0815	2.02794
26	18.1	1.69	13.8465	2.34741
27	19.1	1.96	14.6115	2.72244
28	20.2	2.22	15.453	3.08358
29	21.1	2.48	16.218	3.44472
30	22.1	2.75	16.9065	3.81975
31	23.1	3.02	17.6715	4.19478
32	24.1	3.28	18.4365	4.55592
33	25.1	3.51	19.2015	4.87539
34	26.2	3.78	20.043	5.25042

Table 5.3. Data collected for the Laser Output

Thus,

$$\mathrm{X} = \frac{100}{72}\mathrm{Y} = 1.389\mathrm{Y} \tag{5.4}$$

Using Origin software, the plots of the fiber output and the laser output (in ambient air) are shown in Figure (5.8). The slope efficiencies and the threshold are obtained by using the linear regression equation

$$\mathrm{Y} = \mathrm{A} + \mathrm{B}x, \tag{5.5}$$

with A=-6.20246 ± 0.21073 and B=0.40738 ± 0.01038. The slope efficiency of the fiber, obtained in room temperature (25°C), was 40 % with a threshold of 15.2 W. According to the definition of quantum efficiency[2] with respect to a source of radiant flux, the cross relaxation energy transfer [5, 20] is not observed. In some cases the quantum efficiency of a laser can be larger than unity. This is due to the energy transfer between laser-active ions, which lead to an increase of efficiency from 40.7%, in room temperature, to 47% by cooling the fiber as shown in Figure (5.9) and a decrease of the threshold, from 15.2 W in room temperature to 8.83 W at 0°C. From these measurements, one can say that the thulium

[2]Ratio of emitted photons to the number of photons absorbed

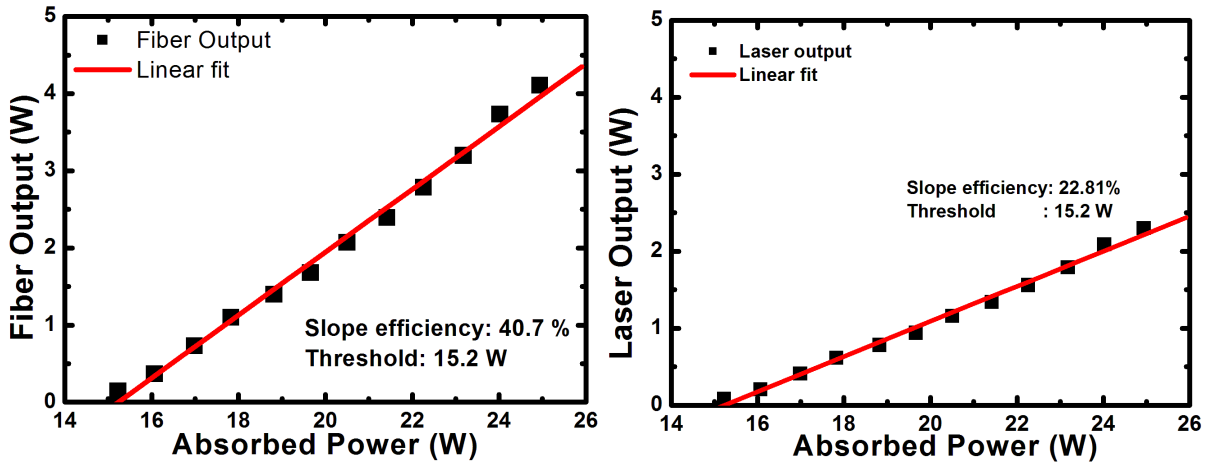

(a) Fiber Output (b) Laser Output

Figure 5.8. Slope efficiencies of thulium doped fiber laser in room temperature

doped fiber is more efficient when it is cooled. The spectrum of the Tm^{3+}-doped fiber was recorded and is shown in Figure (5.10). The plot shows a multi-wavelength emission due to different transitions of the ions to the lower vibrational levels of the ground electronic state $^3H_6$ when it is cooled, according to Boltzmann Statistics distribution on the vibrational population level [39] (see discussion to Figures 5.14 and 5.15).

5.5.2 Efficiencies and spectra of the fiber with un-doped pieces spliced to the ends of Tm^{3+}-doped fiber.

The aim of the experiment was to investigate how the output power and the spectrum of the Tm^{3+}-doped fiber varies with temperature. Using different resonators configurations, the characterization of the fiber was done in room temperature (25°C) and ice water (0°C). Un-doped fiber pieces were spliced to both ends of the fiber to make cooling of the entire active part possible.

Resonator 1: fiber-flat mirror

The resonator 1 is used in the configuration of the experimental setup of Figure (4.1), which consists of a flat mirror in direct contact with the fiber for feedback oscillations. The results of the thulium doped fiber efficiencies and spectra are shown in Figure (5.11).

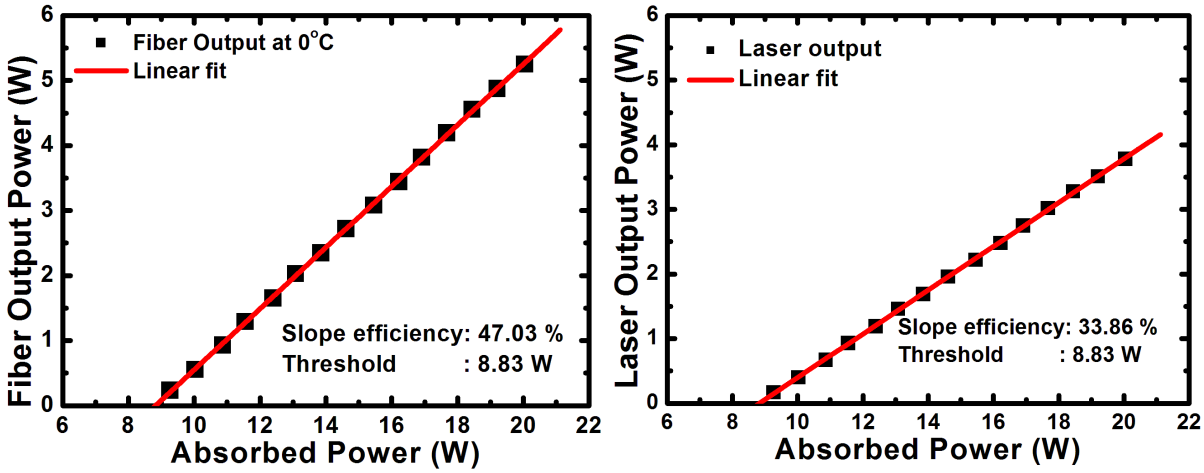

(a) Fiber Output (b) Laser Output

Figure 5.9. Slope efficiencies of thulium doped fiber laser in ice water.

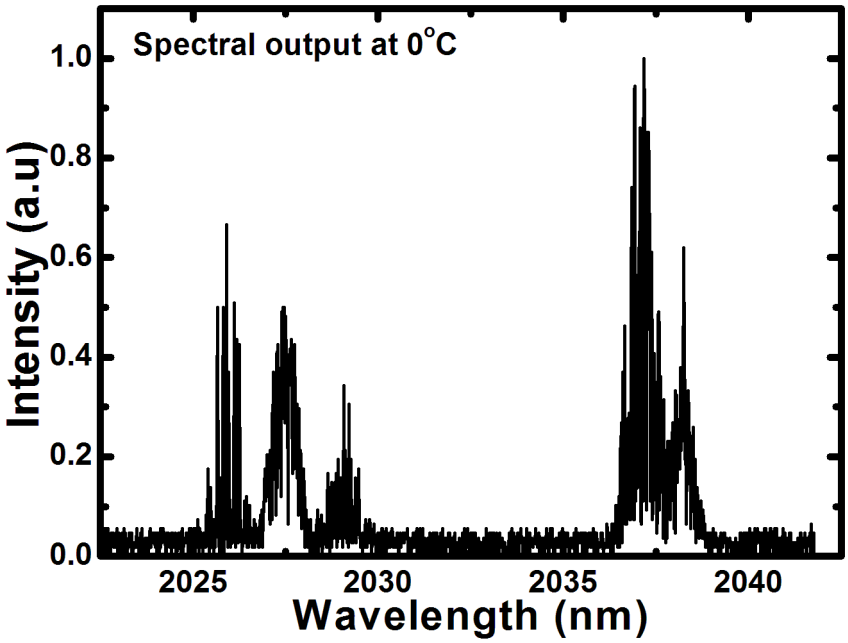

Figure 5.10. Spectral output of the fiber at 0°C

Figures (5.11a and 5.11b) show the fiber output power with respect to the absorbed pump power. The laser starts lasing (threshold) when the absorbed power power reaches the value of 9.9 W (at room temperature) and 7.78 W (at 0°C). The increase of the absorbed power increases the output power of the fiber linearly, this is due to the stimulated emission caused by the injection of the pump power. The gradient above the threshold, gives the

slope efficiencies of the fiber. The slope efficiencies vary with temperature as it is put in different environments. Figure (5.11) shows that the slope efficiency of the fiber is higher in room temperature (53.6%) than when it is cooled with ice water (49.3%). The spectra of the optical output present a multi-mode wavelengths around 2.015 μm, 2.03 μm, and 2.04 μm in ice water and a maximum peak around 2.02 μm in room temperature. There are additional losses in the cavity caused by the spliced junction of the doped fiber (active medium) and the un-doped fiber which serves as the conduction of the pump and signal. The spectral changes between 25°C and 0°C can be explained by noting that cooling changes the gain-loss characteristics of the laser cavity. Since the cavity does not contain wavelength selection, all wavelengths are amplified which experience more gain than losses. The output power of the fiber is limited by the damage threshold of the external cavity.

Resonator 2: fiber-spherical mirror

The resonator 2 is used in the configuration of the experimental setup of Figure (4.13). In this configuration, the feedback for laser oscillations is provided by a spherical mirror with 2.5 cm focal length. The results of the measurements of the efficiencies and spectra of the Tm^{3+}- doped fiber, at 0°C and 25°C, are show in Figure (5.12). As discussed previously, the slope efficiency of the fiber is higher in room temperature than in ice water, as shown in Figures (5.12a) and (5.12b). The decrease in efficiency, compared to the first Tm^{3+}-doped fiber, is caused by the losses provided by coupling back the signal inside the fiber with the spherical mirror. The output spectra are shown in Figures (5.12c) and (5.12d). The peak intensity of the spectra are observed around 2.016 μm in room temperature and ice water. This resonator configuration can become unstable for small changes in length or for small misalignment of the mirror.

Resonator 3: fiber-lens-flat mirror

The experimental setup using the resonator configuration 3 is shown in Figure (4.14). The resonator is made of the fiber, a lens, and a plane mirror. The results of the experimental measurements of the efficiencies and spectra of the thulium doped fiber, in room temperature and ice water, are shown in Figure (5.13). Contrary to the two previous resonator configurations, a slight increase in slope efficiency is observed, 41.3% at room temper-

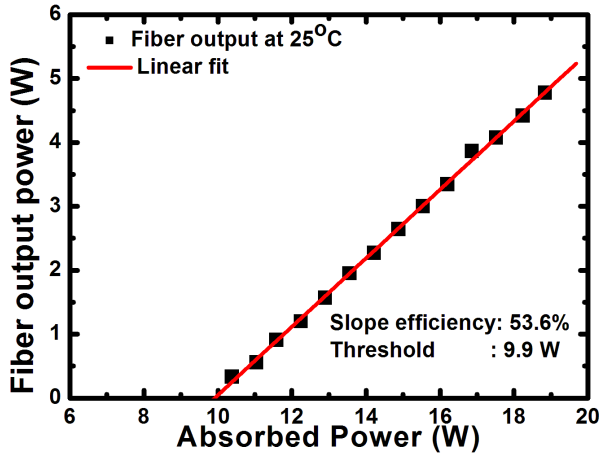

(a) Slope efficiency of the fiber at 25°C.

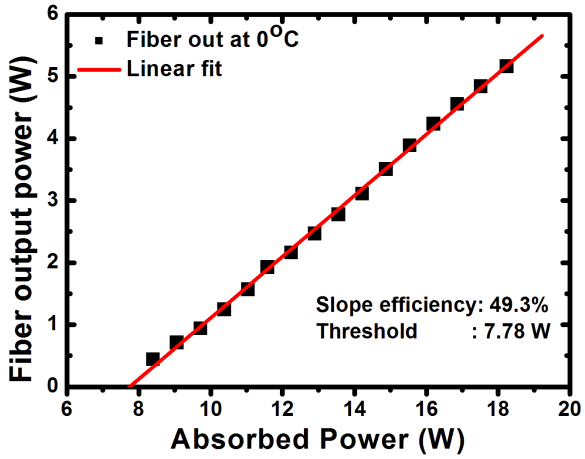

(b) Slope efficiency of the fiber at 0°C.

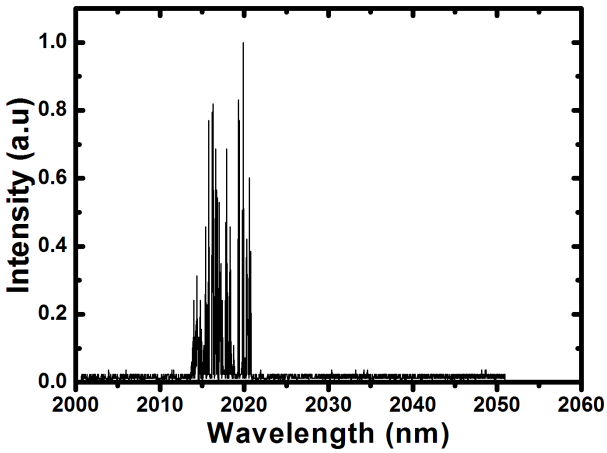

(c) Emission spectrum of the fiber at 25°C.

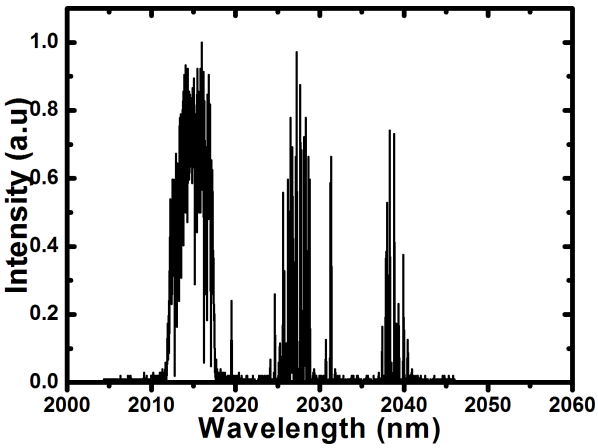

(d) Emission spectrum of the fiber at 0°C.

Figure 5.11. Efficiencies and spectra of the Tm^{3+}-doped fiber with un-doped pieces using the configuration of resonator in Figure (4.1).

ature and 43.2% at 0°C. The spectra observed show multi-wavelengths at 2.02 μm and 2.03 μm in room temperature and the spectrum of the cooled fiber shifts towards shorter wavelengths, as shown in Figures (5.13c) and (5.13d). The decrease of the threshold is observed in all the resonator configurations by cooling the fiber. The shorter wavelengths observed when the fiber is cooled can be explained by using Boltzmann distribution on the vibrational level population. The Boltzmann distribution tells how the internal energy levels of a system is distributed amongst the various energy levels of the system as shown in Figure (5.14a). When the fiber is not pumped, all the ions are in the vibrational levels

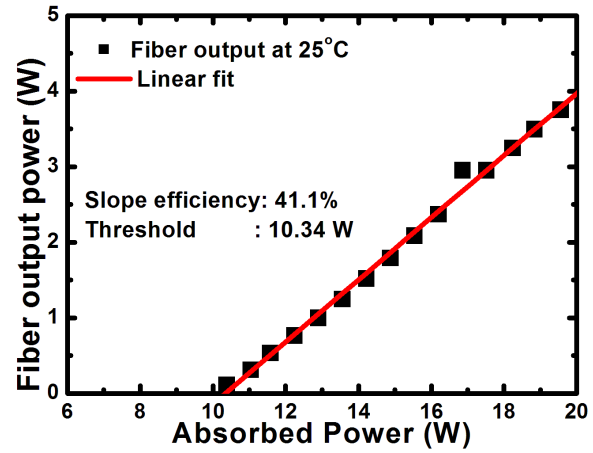

(a) Slope efficiency of the fiber in room temperature

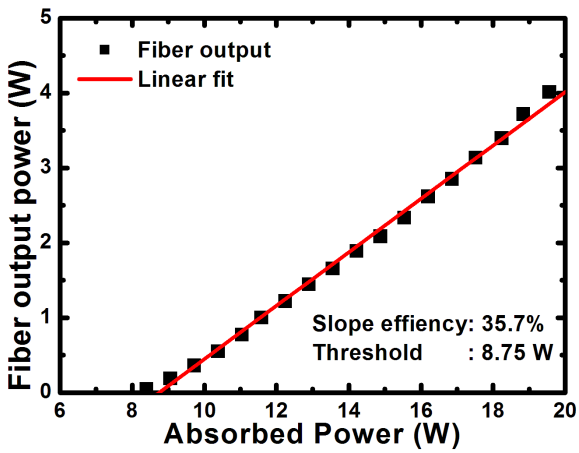

(b) Slope efficiency of the fiber in ice water

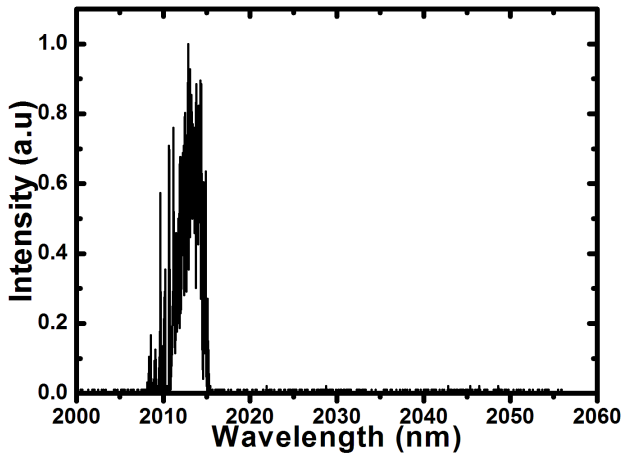

(c) Spectral output of the fiber at 25°C.

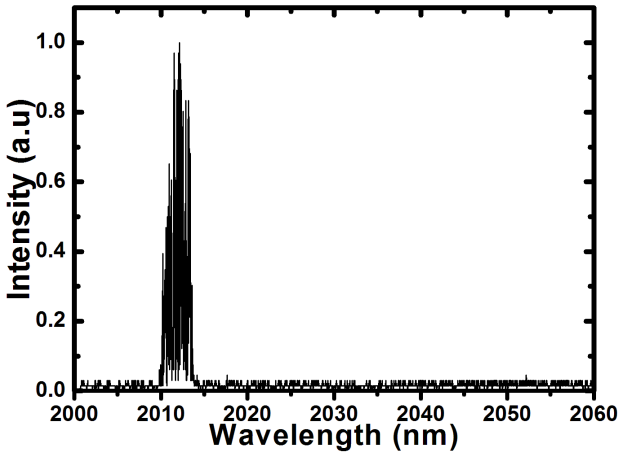

(d) Spectral output of the fiber at 0°C.

Figure 5.12. Efficiencies and spectra of the Tm^{3+}-doped fiber using the configuration of resonator in Figure (4.13).

of the ground electronic state at room temperature. The ground electronic level $^3H_6$ of Tm^{3+}-doped fiber is composed of vibrational energy levels ($\nu = 1, 2, 3, ...$) which are much more closely spaced than the electronic levels. When the fiber is pumped and population inversion occurs at room temperature, the laser transition is done between $^3F_4$ level and the highest vibrational levels because the high vibrational levels are least occupied, thus the longer wavelengths are observed.

When the fiber is cooled, the ions are in the lower vibrational levels of the ground electronic

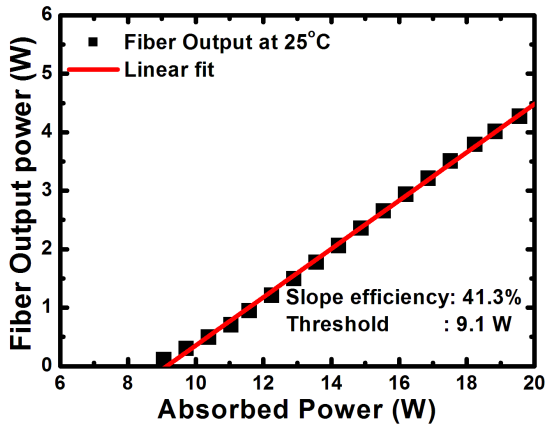

(a) Slope efficiency of the fiber in room temperature

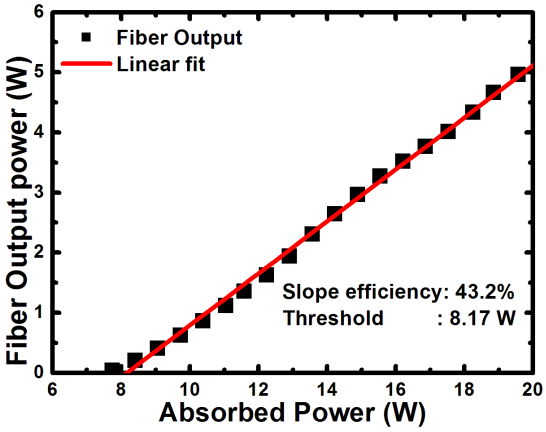

(b) Slope efficiency of the fiber in ice water

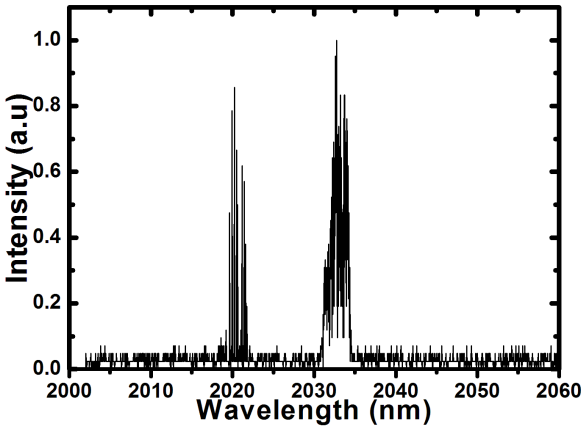

(c) Spectral output of the fiber in room temperature

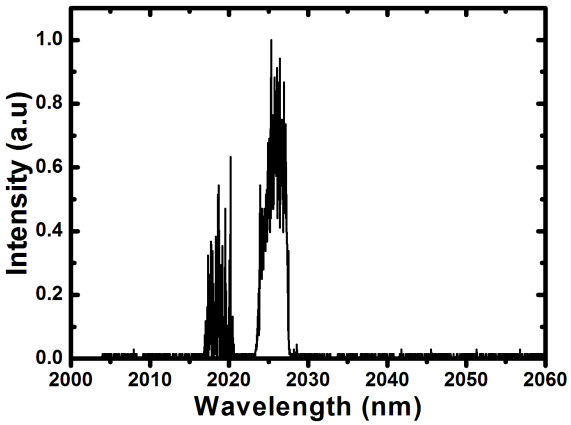

(d) Spectral output of the fiber in ice water

Figure 5.13. Efficiencies and spectra of the Tm^{3+}-doped fiber using the configuration of resonator in Figure (4.14).

state $^3H_6$ as shown in Figure (5.15a). Since all the ions are in the lower vibrational levels, less energy is needed to start population inversion which decreases the threshold. Additionally, the laser transition can now occur to lower vibrational levels of the ground state, thus shorter wavelengths are observed (Figure 5.15b). One can say that the fiber output power is temperature dependent.

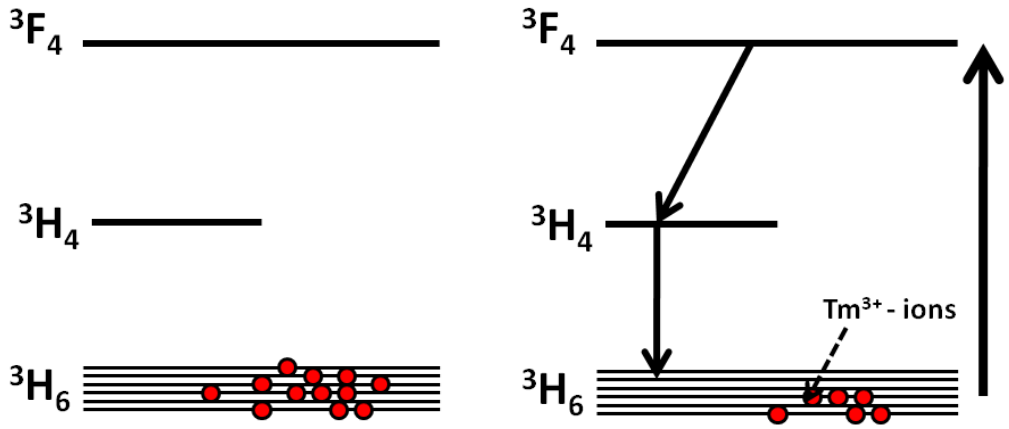

(a) Distribution of ions at room temperature.

(b) Laser emission at 0^o C

Figure 5.14. Boltzmann distribution of Tm^{3+} ions on different vibrational levels.

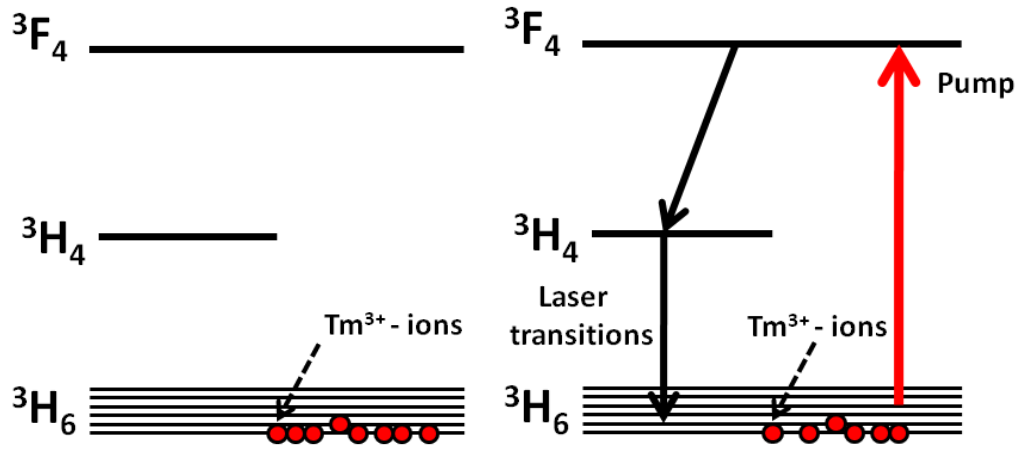

(a) Distribution of ions when the fiber is cooled.

(b) Laser emission at lowest vibrational levels

Figure 5.15. Boltzmann distribution of Tm^{3+} ions on different vibrational levels for a cooled fiber.

5.5.3 High power

The measurements of the efficiencies and spectra of the fiber at high power was done with the resonator configuration 3. The results of the efficiencies and spectrum of the fiber at -15°C, 0°C, and 25°C are shown in Figure (5.16). As the temperature increases, the slope efficiency decreases as shown in Figures (5.16a), (5.16b), and (5.16c). A fiber output power

of 10 W with 30 W of absorbed power was measured. The maximum output power of the diode laser was not used to pump the fiber because the maximum input current that the available power supply can support was 55 A, which corresponds to an absorbed power of 31.7 W. The spectral output is shown in Figure (5.16d). The peak intensities are around 2.02 μm and 2.035 μm.

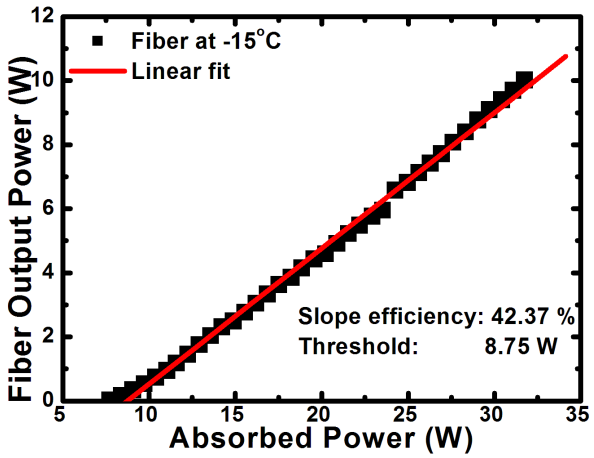

(a) Fiber output power versus absorbed pump power at −15°C. The slope efficiency is 42.37% with respect to the absorbed power.

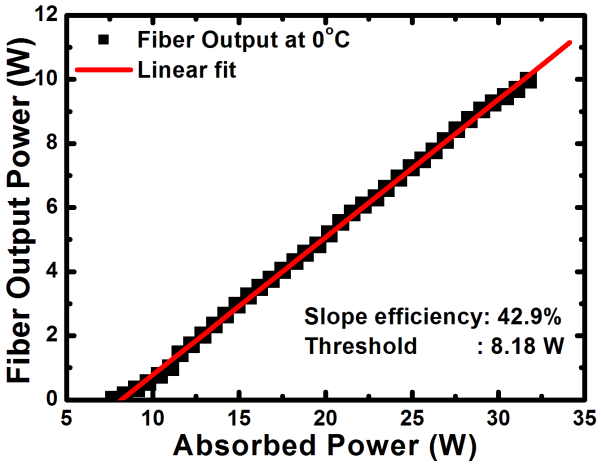

(b) Slope efficiency of the fiber in ice water

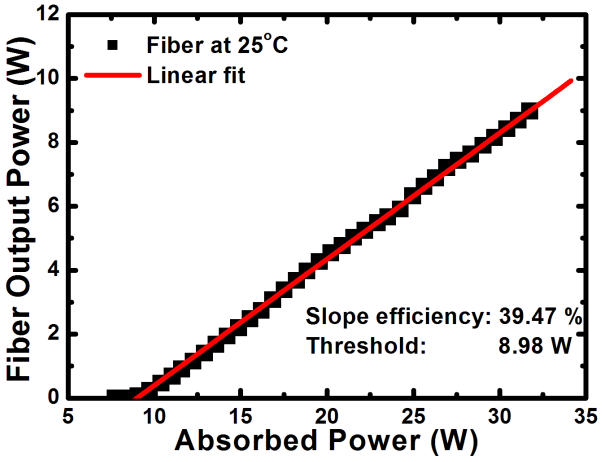

(c) Slope efficiency of the fiber at 25°C.

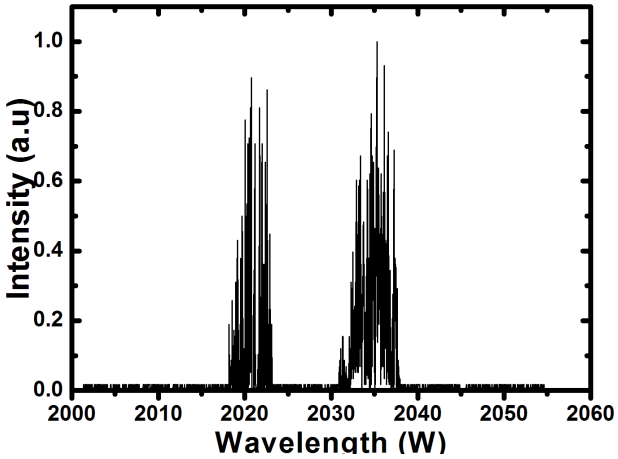

(d) Emission spectrum of the fiber at high power at −15°C.

Figure 5.16. Efficiencies and spectrum of the Tm^{3+}-doped fiber at high power.

5.6 Comparison

This section illustrates the comparison of the efficiencies of the two Tm^3-doped fiber used. Figures (5.17a) and (5.17b) show the results of efficiencies measurements of the fibers at 25°C and 0°C, with the configuration of Figure (4.1). From the legend, the first fiber is the Tm^3-doped fiber without un-doped fibers spliced at the ends of the doped fiber. At room temperature, the fiber with spliced end pieces has a significantly lower threshold. Without the end pieces, a part of the active fiber must be kept outside the cooling water for the pump coupling. This part heats up and reduces efficiency considerably. With the end pieces, the heat created in the active part can be extracted more efficiently. When the fiber is cooled, the fibers behave very similar. The decreased slope efficiency for the fiber with end pieces can be attributed to losses occurring at the spliced connections.

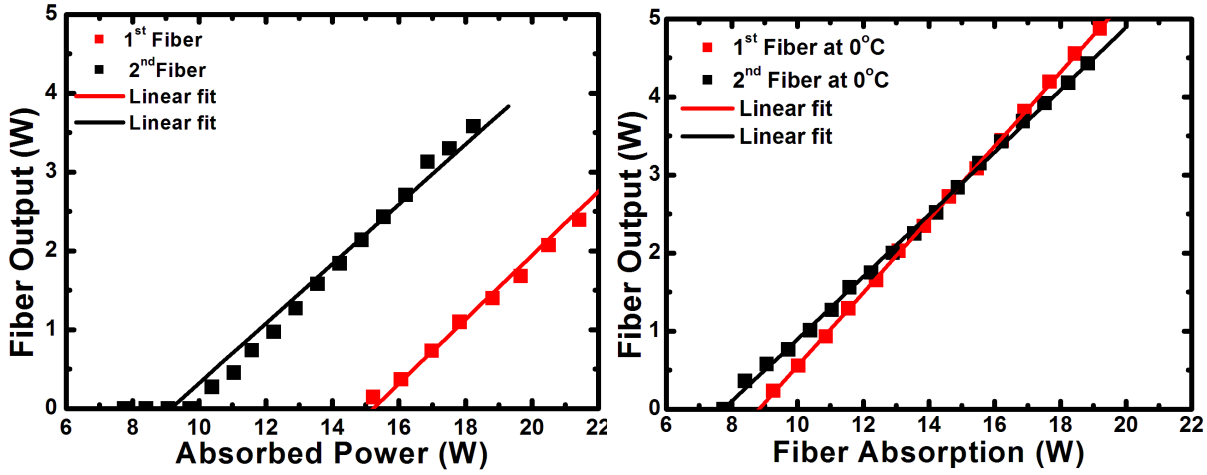

(a) Efficiencies of Tm^{3+} fiber at 25°C. (b) Efficiencies of Tm^{3+} fiber at 0°C.

Figure 5.17. Comparison of the efficiencies of the two Tm^{3+}-doped fibers used at 25°C and 0°C.

Chapter 6

Conclusion

6.1 Summary

In this thesis, the characterization of a newly developed Tm-doped fibers, manufactured by CorActive, have been studied. The work included theory on the propagation of light through an optical waveguide, theory on rare earth elements and thulium-doped fiber as an amplifier for laser systems. Experimentally, the characterization of the pump diode and mirrors have been studied to optimize the laser resonator length. The diode laser was tuned to operate at 800 nm because Tm-doped fibers possess strong absorption features around $780 - 800$ nm, allowing for incorporation of the laser gain material and the pump delivery system in double clad fiber [40]. Simple setups were designed for the study of the Tm-doped fiber as shown in Figures (4.1), (4.13), and (4.14), and optimal length of 4 m of the fiber was used for the resonator length. The experimental characterization was the determination of the slope efficiency and spectral output of the fiber, when pumped with commercial diode laser. During this study, the characterization of the Tm-doped fiber has been done using different cooling techniques, such as cooling the fiber at 0°C with ice water and -15°C with salt+ice water.

Two different fiber configurations, with the same concentration of thulium ions (5 wt%), was used. The first fiber used has 4 m length of active medium and the second has 4 m of active medium but was spliced at both ends of the fiber with un-doped fiber for the transmission of pump light and signal, and also to facilitate the active medium to be

placed in a cooled compartment. Slope efficiencies of 40.7% and 47% were obtained at room temperature (25°C) and in ice water (0°C), respectively, with an emission spectrum ranging from $2.02-2.04$ μm. An output power of 5 W (with 20 W of absorbed power) was obtained. During the study of the first fiber, the maximum output power was limited by the damage threshold of the external cavity. An efficiency of 53%, with an output power of 5 W, and a spectra ranging from $2.02-2.04$ μm was obtained using the second fiber. The study of the second fiber shows that as the temperature decreases, the slope efficiency of the fiber decreases, this is due to the losses at the spliced junctions. It is difficult, but not impossible, to determine the losses at the spliced simply because we do not have the right optics to do the measurements.

The experimental measurements were also done at high power. The maximum output power of the diode laser could not be used because of the damage threshold of power supply and the external cavity of the laser.

The "two-for-one" cross relaxation phenomenon was observed and the spectral output of the fiber is ranging from $2.01-2.04$ μm as expected.

We have produced, at high power, a CW output power of 10 W at -15°C and 0°C (32 W of absorbed power) from a diode-cladding-pumped Tm^{3+}-doped silica fiber laser that operated a slope efficiency of 42.37% at -15°C, 42.9% at 0°C, and 39.47% at room temperature and spectral output with multi-wavelengths around 2.02 μm and 2.04 μm. For three-level or quasi-three-level systems, such as Tm^{3+} and Er^{3+}, longer fiber will result in considerable re-absorption and therefore lead to high threshold and low efficiency [41, 42]. To reduce re-absorption, intense pump power should be maintained in the fiber to keep the population inversion relatively high.

This laser finds its applications on the bio-medical area, in gas sensing. It can be used for pumping Mid-IR lasers, for eye-safe radar and LIDAR, and other military applications.

6.2 Future work

We believe that the efficiency of Tm^{3+}-doped fiber can be improved by optimizing the doping concentration and laser length, by using other cooling techniques such as liquid

nitrogen and suitable optics for 2 μm.

Appendix A

Decibels

A.1 Decibels

In designing and implementating an optical fiber link, it is of interest to establish, measure, and/or interrelate the signal levels at the transmitter, at the receiver, at the cable connection and splice points, and in the cable. A convenient method for this is to reference the signal level either to some absolute value or to a noise level. This is normally done in terms of power ratio measured in *decibels* (dB) defined as

$$\text{Power ratio in dB} = 10 \log \frac{P_2}{P_1} \tag{A.1}$$

where P_1 and P_2 are electric or optical powers.

The logarithmic nature of the decibel allows a large ratio to be expressed in a fairly simple manner. Power levels differing by many orders of magnitude can be simply compared when they are in decibel form. Some very helpful figures to remember are given in Table (A.1). For example, doubling the power means a 3-dB gain (the power level increases by 3 dB), halving the power means a 3-dB loss (the power level decreases by 3 dB), and power levels differing by factors of 10^N or 10^{-N} have decibel differences of $+10N$ dB and -10N dB, respectively.

Table A.1. Examples of decibel measures of power ratios

Power ratio	10^N	10	2	1	0.5	0.1	10^{-N}
dB	+10N	+10	+3	0	-3	-10	-10N

A.2 The decibel meter (dBm)

The decibel is used to refer to ratios or relative units. For example, we can say that a certain optical fiber has a 6-dB loss (the power level gets reduced by 75 percent in going through the fiber) or that a particular connector has a 1-dB loss (the power level gets reduced by 20 percent at the connector). However, the decibel gives no indication of the absolute power level. One of the most common derived units for doing this optical fiber communications is the dBm. This is the decibel power level referred to 1 mW. In this case, the power in dBm is the absolute value defined by

$$\text{Power level} = 10 \log \frac{P}{1 \text{ mW}} \tag{A.2}$$

An important relationship to remember is that 0 dBm = 1 mW. Other examples are shown in Table (A.2).

Table A.2. Examples of dBm units (decibel measure of power relative to 1 mW)

Power (mW)	100	10	2	1	0.5	0.1	0.01	0.001
Value (dBm)	+20	+10	+3	0	-3	-10	-20	-30

Bibliography

[1] C. Scott , G. Frith, and B. Samson. Developments in thulium-doped fiber lasers offer high powers. *SPIE Newsroom*, 2008.

[2] Matlab Central. Optical Fiber Toolbox, http://www.mathworks.com/matlabcentral/fileexchange/2 optical-fibre-toolbox.

[3] Jenoptik. Lasers and Material Processing, http:/www.jenoptik.com/diodelasers.

[4] PerkinElmer. Perkin Elmer Lambda 9 UV/VIS/NIR Spectrophotometer, http://www.monoinstruments.com/pe9.html.

[5] G.A. Slobodtchikov E.V. Wall K.F. Frith G. Samson B. Carter A.L.G. Moulton, P.F. Rines. Tm-doped fiber lasers: Fundamentals and power scaling. *Selected Topics in Quantum Electronics, IEEE Journal of*, 15(1):85–92, Jan. 2009.

[6] Terence A. King Stuart D. Jackson. High-power diode-cladding-pumped Tm-doped silica fiber laser. *Opt. Lett.*, 23(18):1462–1464, 1998.

[7] J.L. Hanna D.C. Reekie L. Russell P.S.J. Townsend J.E. Tropper A.C. Pask, H.M. Archambault. Operation of cladding-pumped Yb^{3+}-doped silica fibre lasers in 1 μm region. *Electronics Letters*, 30(11):863 –865, 26 1994.

[8] C. A. Codemard J. Nilsson J. K. Sahu D. N. Payne R. Horley P. W. Turner L. M. B. Hickey A. Harker M. Lovelady A. Piper Y. Jeong, S. Yoo. Erbium:Ytterbium codoped large-core fiber laser with 297-W continuous-wave output power. *IEEE Journal on Selected Topics in Quantum Electronics*, 13(3):573–579, 05 2007.

[9] R.J. Sutton S.B. Speth J.A. Mitchell S.C. Skidmore J.A. Emanuel M.A. Payne S.A. Honea, E.C. Beach. 115-W Tm:YAG diode-pumped solid-state laser. *Quantum Electronics, IEEE Journal of*, 33(9):1592 –1600, sep 1997.

[10] W. Weber H.P. Vlasov V.I. Zavartsev Y.D. Studenikin P.A. Zagumennyui A.I. Shcherbakov I.A. Wyss, C.P. Luthy. A diode-pumped 1.4-W Tm^{3+}:$GdVO_4$ microchip laser at 1.9 μm. *Quantum Electronics, IEEE Journal of*, 34(12):2380 –2382, Dec 1998.

[11] M.C. Teich B.E.A.Saleh. *Fundamentals of PHOTONICS*. Wiley, 2007.

[12] G. Agrawal. *Nonlinear Fiber Optics*. Academic Press, 3 edition, January 2001.

[13] Rutger W. Smink Bastiaan P. de Hon Anton G. Tijhuis. Bending loss in optical fibers—a full-wave approach. *J. Opt. Soc. Am. B*, 24(10):2610–2618, Oct 2007.

[14] Alexander Argyros Richard Lwin Maryanne C. J. Large. Bend loss in highly multimode fibres. *Opt. Express*, 16(23):18590–18598, Nov 2008.

[15] E.l Wolf M. Born. *Principles of Optics*. Cambridge University Press, 1999.

[16] Michel J.F. Digonnet. *Rare-Earth-Doped Fiber Lasers and Amplifiers, Second Edition, Revised and Expanded (Optical Engineering)*. CRC, 2001.

[17] Nissan Spector. Spectroscopic Properties of Rare Earths. Brian G. Wybourne. Interscience (Wiley), New York, 1965. x + 236 pp. Illus. 10.50. *Science*, 148(3673):1082–, 1965.

[18] R. Segre J. Snitzer, E. Woodcock. Phosphate glass Er^{3+} laser. *Quantum Electronics, IEEE Journal of*, 4(5):360 – 360, may. 1968.

[19] Frith G, D. G. Lancaster, S. D. Jackson. 85 W Tm^{3+} -doped silica fibre laser. *Electronics Letters*, 41(12):1 – 2, 2005.

[20] S. D. Jackson, S. Mossman. Efficiency dependence on the Tm^{3+} and Al^{3+} concentrations for Tm^{3+}-doped silica double-clad fiber lasers. *Appl. Opt.*, 42(15):2702–2707, 2003.

[21] Mary Elvira Weeks. The discovery of the elements. xvi. the rare earth elements. *Journal of Chemical Education*, 9:1751–1773, October 1932.

[22] Jefferson Lab. Thulium element, http://education.jlab.org/itselemental/ele069.html.

[23] Vikas Sudesh J. A. Piper E. M. Goldys R. S. Seymour. Growth, characterization, and laser potential of Tm:$La_2Be_2O_5$. *J. Opt. Soc. Am. B*, 15(1):239–246, 1998.

[24] J.E. Barnes, W.L. Townsend. Highly tunable and efficient diode pumped operation of Tm^{3+}-doped fibre lasers. *Electronics Letters*, 26(11):746 –747, 24 1990.

[25] I.M. Percival R.M. Perry I.R. Smart R.G. Suni P.J. Townsend J.E. Tropper A.C. Hanna, D.C. Jauncey. Continuous-wave oscillation of a monomode thulium-doped fibre laser. *Electronics Letters*, 24(19):1222 –1223, 15 1988.

[26] D.C. Hanna R.M. Percival R.G. Smart A.C. Tropper. Efficient and tunable operation of a Tm-doped fibre laser. *Optics Communications*, 75(3-4):283 – 286, 1990.

[27] E. Allain J.Y. Bayon J.F. Niay P. Bernage P. Boj, S. Delevaque. High efficiency diode pumped thulium-doped silica fibre lasers with intracore bragg gratings in the 1.9-2.1 μm band. *Electronics Letters*, 30(13):1019 –1020, jun. 1994.

[28] Anne C. Tropper Richard G. Smart Ian R. Perry David C. Hanna John R. Lincoln William S. Brocklesby. Thulium-doped silica fiber lasers. volume 1373, pages 152–157. SPIE, 1991.

[29] S. D. Jackson. Cross relaxation and energy transfer upconversion processes relevant to the functioning of 2 μm, Tm^{3+} -doped silica fiber lasers. *Optics Communication*, 230:197–203, 2004.

[30] Y. Komukai T. Yamamoto, T. Miyajima. 1.9 μm Tm-doped silica fibre laser pumped at 1.57 μm. *Electronics Letters*, 30(3):220 –221, 3 1994.

[31] Jianfeng Wu Zhidong Yao Jie Zong Shibin Jiang. Highly efficient high-power thulium-doped germanate glass fiber laser. *Opt. Lett.*, 32(6):638–640, 2007.

[32] Jenoptik. Jenoptik specification sheet, http://www.jenoptik.com.

[33] CorActive. Datasheet of thulium absorption spectrum, http://www.coractive.com/, 2009.

[34] Division of Fisher Scientific Co. Instruction manual: Model $82-000$ Series 0.5 Meter Ebert Scanning Spectrometer. *Jarrell-Ash*, 1971.

[35] Grossman William E. L. The optical characteristics and production of diffraction gratings: A quantitative explanation of their experimental qualities with a description of their manufacture and relative merits. *Journal of Chemical Education*, 70(9):741, 1993.

[36] Demtroder Wolfgang. *Laser spectroscopy, 3rd edition : basic concepts and instrumentation / Wolfgang Demtroder*. Springer-Verlag, Berlin ; New York, 2002.

[37] Thorlabs. Datasheet of DET10D detector, http://www.thorlabs.com.

[38] Encyclopedia of Laser Physics & Technology. Laser threshold. *http: //www.rp-photonics.com*.

[39] Orazio Svelto. *Principles of Lasers*. Springer Science+Business Media, Inc., 1998.

[40] N. P. Walsh, B. M. Barnes. Comparison of Tm : ZBLAN and Tm : silica fiber lasers; spectroscopy and tunable pulsed laser operation around 1.9 μm. *Applied Physics B: Lasers & Optics*, 78(3/4):325 – 333, 2004.

[41] T.Y. Fan. Optimizing the efficiency and stored energy in quasi-three-level lasers. *Quantum Electronics, IEEE Journal of*, 28(12):2692 –2697, Dec 1992.

[42] I. Kelson and A. Hardy. Optimization of strongly pumped fiber lasers. *Lightwave Technology, Journal of*, 17(5):891 –897, May 1999.